Ville Väliaho

Modelling and Simulation of an IPMSM-motor

Metropolia University of Applied Sciences

Bachelor of Engineering

Automotive Engineering

Bachelor's Thesis

7 April 2025

Abstract

Author:	Ville Väliaho
Title:	Modelling and Simulation of an IPMSM-motor
Number of Pages:	56 pages
Date:	7 April 2025
Degree:	Bachelor of Engineering
Degree Programme:	Automotive Engineering
Professional Major:	Automotive Electrics
Supervisors:	Pasi Kovanen, Senior Lecturer

This thesis describes the measurements, modelling and simulations of an interior permanent magnet synchronous motor. The goal was to produce a FEM model that accurately matches the parameters listed in the motor's datasheet.

The measurements included all the necessary geometries that had to be modelled as well as winding layout and material properties. The measurements were done with appropriate tools such as a profile projector, micro-meter, calibres, XRF-analyser and a gaussmeter.

Modelling and simulations were made with Ansys RMxprt and Ansys Maxwell. The model was created in a 2D environment and simulations were done with magnetostatic and transient solution types.

The results included field overlays and plots of produced magnetic fields, cogging and steady state torque, induced voltages, flux linkages, input currents and losses. The results were evaluated and further development as well as model usage suggestions were introduced.

Keywords: Electric motor, magnetism, Ansys Maxwell, FEM

Tiivistelmä

Tekijä:	Ville Väliaho
Otsikko:	IPMSM-moottorin mallinnus ja simulointi
Sivumäärä:	56 sivua
Aika:	7.4.2025
Tutkinto:	Insinööri (AMK)
Tutkinto-ohjelma:	Ajoneuvotekniikka
Ammatillinen pääaine:	Autosähkötekniikka
Ohjaajat:	Lehtori Pasi Kovanen

Tämä opinnäytetyö esittelee sisäisen kestomagneettitahtimoottorin mittaukset, mallinnuksen ja simuloinnin. Työn tavoitteena oli tuottaa FEM-malli, joka kuvastaa datalehdessä olevaa moottoria mahdollisimman tarkasti.

Mittaukset sisälsivät kaikki moottorin mallintamiseen vaadittavat geometriat sekä käämien topologian ja materiaalien ominaisuuksia. Mittaukset suoritetiin profiiliprojektorilla, mikrometrillä, työntömitalla, XRF-analysaattorilla ja gaussmetrillä.

Mallinnus ja simulointi toteutettiin Ansys RMxprt- sekä Ansys Maxwell -ohjelmilla. Malli luotiin 2D-ympäristöön ja simulaatiot toteutettiin magnetostaattisissa ja liikkuvissa ratkaisumalleissa.

Työn tulokset sisälsivät kenttäkuvia ja graafeja magneettikentistä, vääntövärähtelyistä, vakaan tilan vääntömomentista, indusoiduista jännitteistä, käämivoista, syöttövirroista ja häviöistä. Tulokset arvioitiin ja mallin jatkokehitys- sekä hyödyntämiskehotuksia esiteltiin.

Avainsanat: Sähkömoottori, magnetismi, Ansys Maxwell, FEM

Contents

List of Abbreviations

FS:	Formula Student
TSAC:	Tractive System Accumulator Container
IPMSM:	Interior Permanent Magnet Synchronous Motor
RPM:	Revolutions Per Minute
FEM:	Finite Element Method
BEMF:	Back Electromotive Force
AWG:	American Wire Gauge
XRF:	X-ray Fluorescent
VSM:	Vibrating-Sample Magnetometer
MMF:	Magnetomotive force
SPP:	Slots per pole per phase
EMF:	Electromotive force
FEA:	Finite element analysis

1 Introduction

This thesis discusses an electromagnetic simulation made of an interior permanent magnet synchronous motor used in Metropolia Motorsport's Formula Student vehicle in the seasons 21-24. The thesis covers the reverse engineering of the motor, modelling of the motor model, simulation setup and results as well as further development suggestions.

The reverse engineering portion covers what preliminary data was available and what was self-measured and eventually inputted for the simulation software. This includes the measurements of geometries, magnetic properties and winding layout.

The simulation itself was conducted with Ansys Maxwell and modelling with Ansys RMxprt. 2D simulation was used and a steady state rated speed simulation was the main point of interest.

With comparison of the simulation results and the data provided by the motor manufacturer, the validity of the simulation was evaluated, and some further development suggestions were presented.

1.1 Formula Student

Formula Student is an international competition for students of universities and universities of applied sciences. The goal of the competition is for each team to design and manufacture a small formula type vehicle to compete in static and dynamic events in different competitions around the world.

The competition officials regulate the rules in terms of vehicle design, permitted and required materials, as well as obligatory testing on the vehicle. A relevant example in this thesis is the maximum allowed power used by the powertrain, which is 80 kW. This is measured at the outlet of TSAC (Tractive System Accumulator Container). (Formula Student Rules 2024: 81.)

1.2 Metropolia Motorsport

Metropolia Motorsport is the FS (Formula Student) team of Metropolia University of Applied Sciences. The team was founded in 2000, and it has been competing ever since. The team moved from combustion vehicle class to EV (Electric Vehicle) class in 2013. The team is run completely by students most of which come from automotive, mechanical and electrical engineering degree programs.

The team's operation is sponsored by various companies most of which provide the necessary products and materials to make it possible to assemble the vehicle. A new vehicle is produced nearly every year with some changes to the previous year's model. The team also produces many of its parts inhouse with CNC (Computer Numerical Control) machines located at the team's home campus at Metropolia. In figure 1, the team's season 23 vehicle HPF023 can be seen.

Figure 1. HPF023 vehicle in FS-Italy in 2023.

1.3 IPMSM-motor

The motor in question in this thesis is the tractive motor used in Metropolia Motorsport's vehicle. The vehicle inherits four in-wheel motor-transmission packages. In figure 2, the cross-section of the motor-transmission package from the team's season 23 vehicle can be seen. The motor-transmission package was designed by the author.

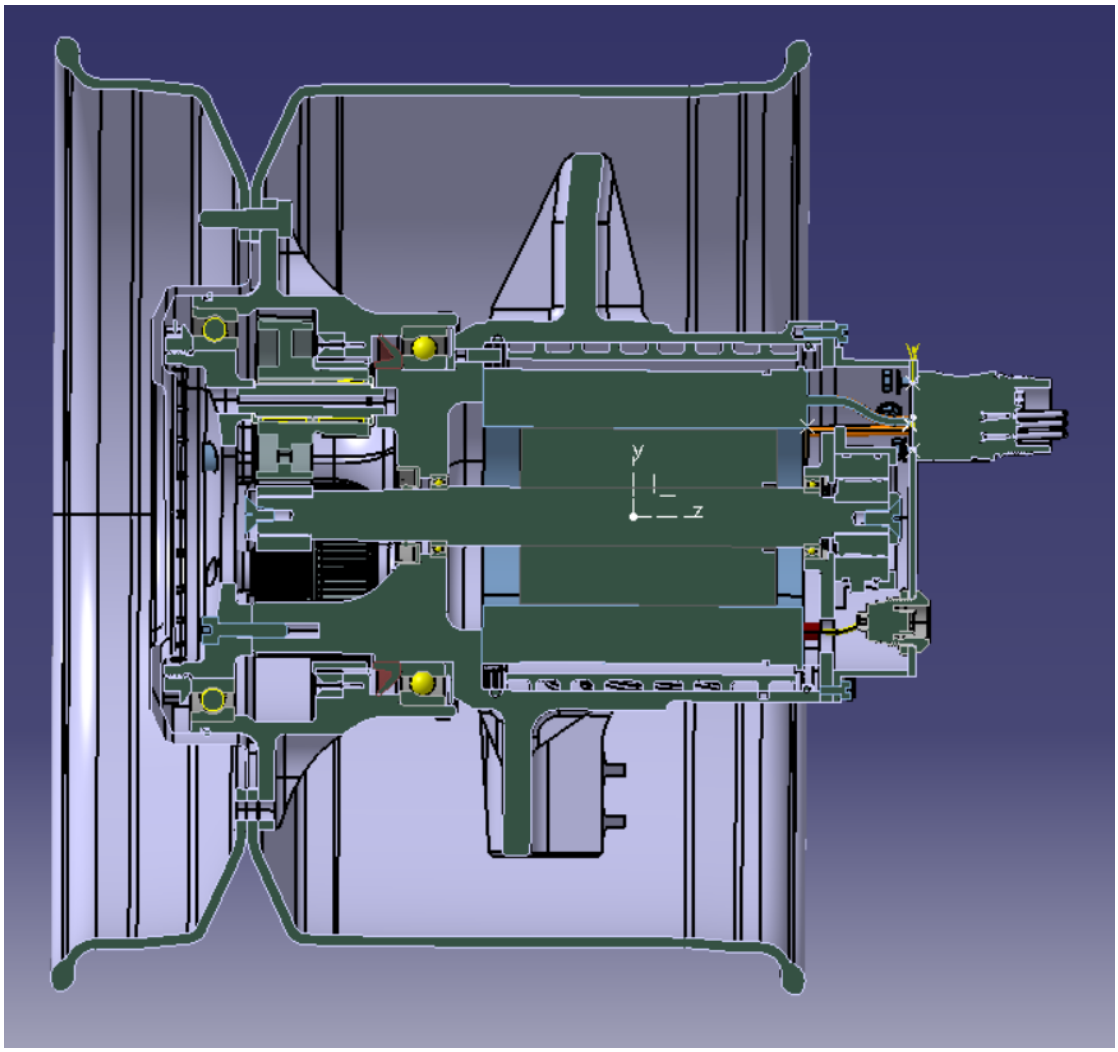

Figure 2. Cross-section of a motor-transmission package of HPF023 modelled in Catia V5.

The motor used is an IPMSM (Interior Permanent Magnet Synchronous Motor). Typically, in PMSMs the permanent magnets are surface mounted on to the rotor, but in an IPMSM the magnets are placed inside the rotor core material embedded into their dedicated slots.

The motor has a rated speed of 13250 rpm (revolutions per minute), rated power of 15404 Watts, and rated torque of 11,1 Nm at rated current of 22,6 Amps (rms). It has a peak torque of 29,1 Nm at peak current of 61 Amps (rms), peak power of 35366 Watts, and a maximum speed of 20000 rpm with field

weakening. The motor manufacturer and exact model is purposely left out due to the manufacturer confidentiality requirements.

Even with IPMSM motors, there are various different ways one can setup the magnets, where each setup has their advantages and disadvantages. For example, the team's motor is a so-called spoke-type IPMSM. This means that the magnets are circumferentially excited. The rotor in question is visible in figure 3 with the N and S letters indicating the orientation of the magnet poles. These represent the path of the flux inside the magnet.

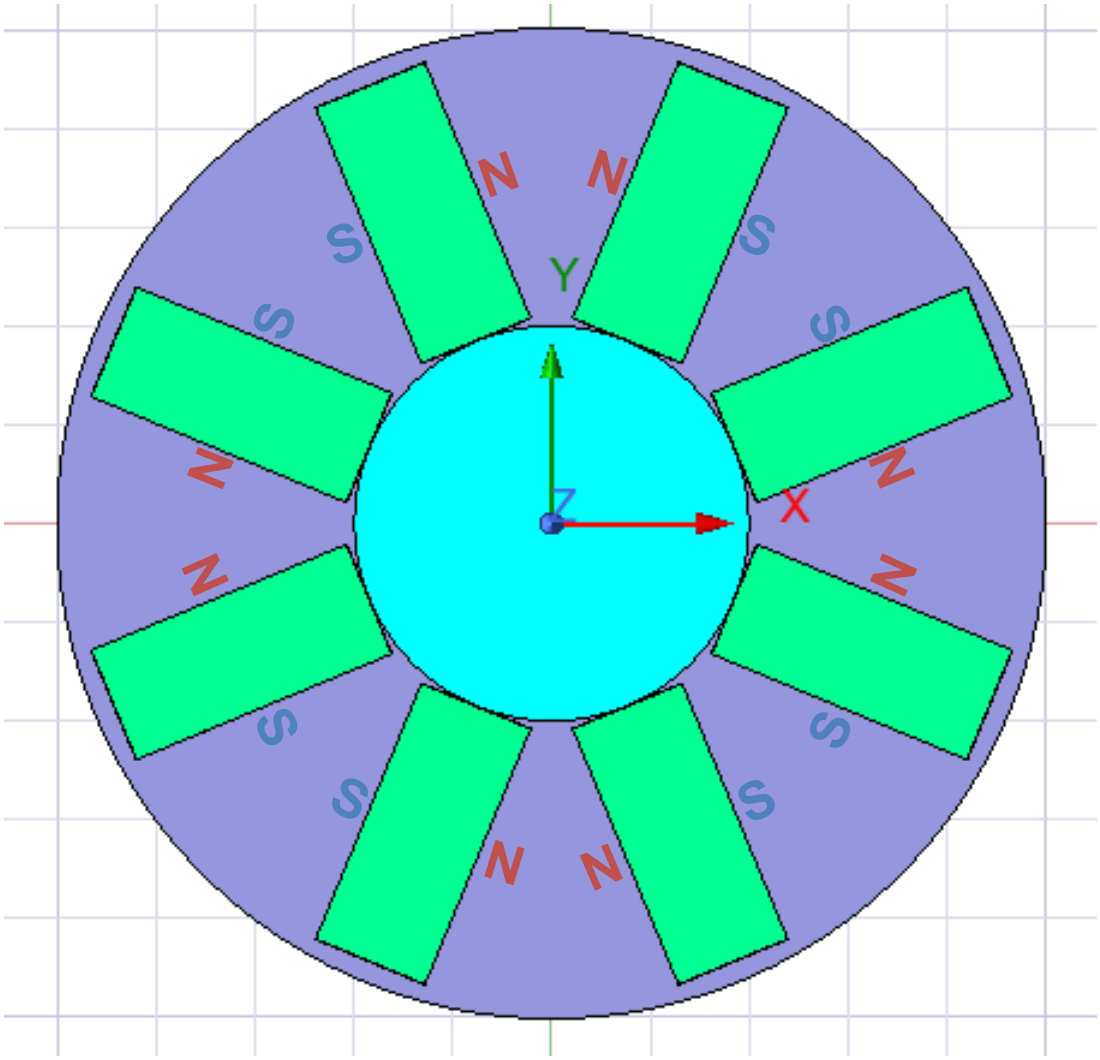

Figure 3. Spoke-type permanent magnet rotor in 2D.

The rotor in figure 3 represents the one in the motor used by the team. As can be seen, the motor is an 8-pole motor. This will be visualized with the simulation in section 6.2.

The stator of the motor is a 12-slot with a concentrated 3-phase copper winding. The stator of the motor is essentially the non-moving part of the motor which is mounted permanently on the chassis or in this case to the wheel knuckle. Its purpose is to hold the windings and to create a path for flux created by the windings and permanent magnets as well as the mounting of the motor. The stator of the team's motor is represented in figure 4.

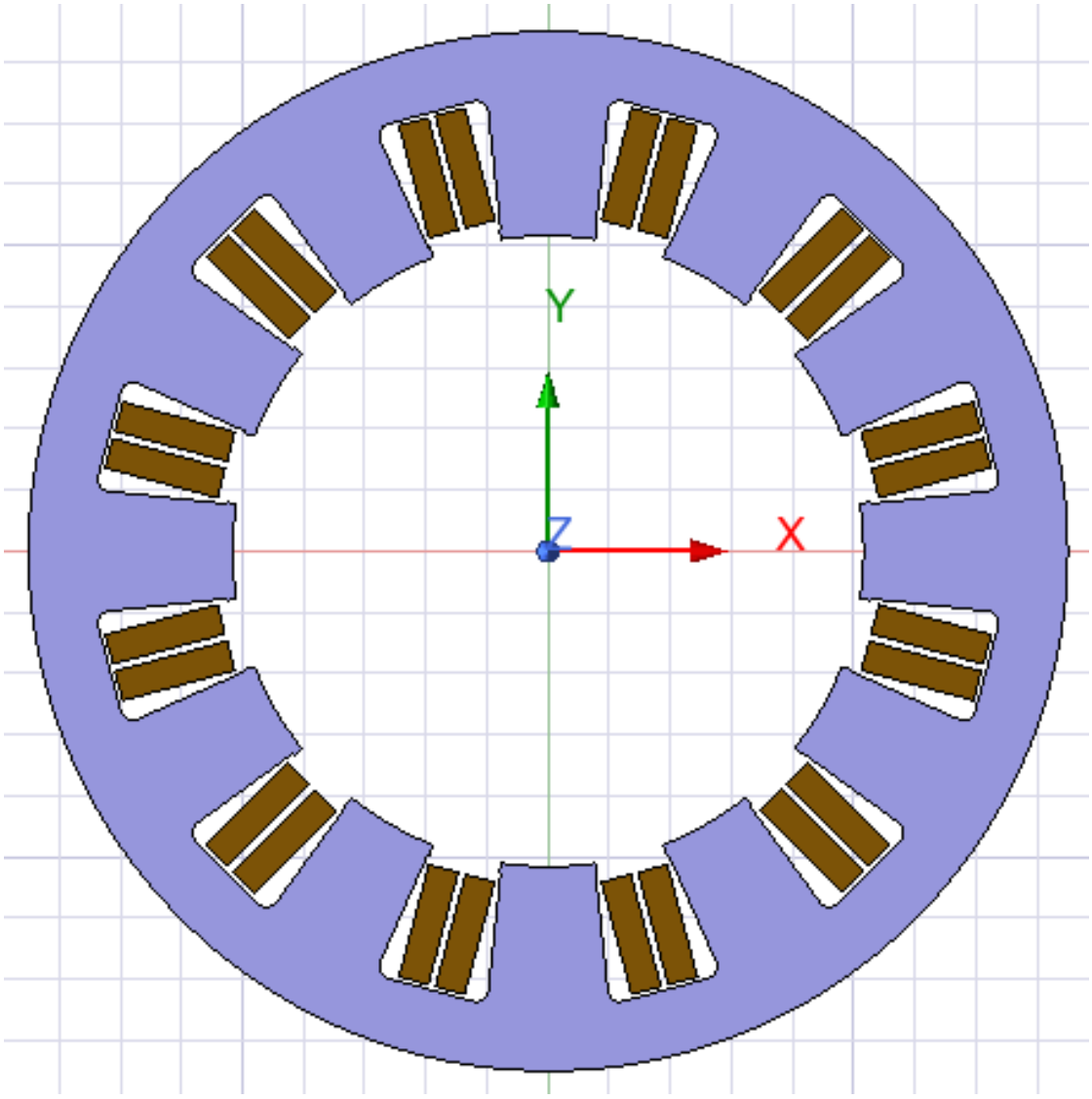

Figure 4. The stator with the windings in 2D.

For the reader to understand the size of the motor, the outer diameter of the stator seen in figure 4 is 85 mm and the length is 70 mm. In figure 4, the blue part represents the stator core-material and the brown rectangles are the cross-sections of the windings circling the stator teeth.

2 Ansys Maxwell

The simulation was executed with Ansys Maxwell. Ansys itself is an American software producer that has been developing modelling and simulation software for various applications since 1970. They are perhaps best known for their CFD (Computational Fluid Dynamics) simulation applications, but they offer very comprehensive electrical simulation applications as well, one of which is the Ansys Maxwell.

Maxwell is essentially an electromagnetic field solver, used to simulate electric motors of all kinds, power electronics and wireless charging. In Maxwell, it is possible to simulate both DC and AC solutions in 2D and 3D environments. The solution types are split into magnetic and electric. The magnetic solution offers three different types of solutions: Magnetostatic, Eddy Current and Transient. The electric solution offers electrostatic, AC Conduction and DC conduction. In this case, the magnetostatic and transient solutions from the magnetic solution type were used. (Ansys Maxwell 2025.)

Magnetostatic solver is used for solving stationary magnetic fields. It allows the user to solve magnetic fields caused by either permanent magnets or DC currents. It is very useful for calculating the flux paths and densities caused by a stationary permanent magnet to see how, for example, the core material saturates. It can also calculate torque caused by the permanent magnet at different rotor positions by sweeping the rotor by a set angle and doing independent computation for each angle step.

Transient solver on the other hand is used to solve time-varying fields. This allows the user to input a rotational velocity to the rotor as well as AC current or

voltage excitation to the windings allowing the user to calculate parameters such as moving torque, induced voltages and D- and Q -axis currents. All three of the magnetic solvers can account for nonlinear material properties as well. (Ansys Maxwell Getting Started 2020.)

3 Measurements

In this chapter, all the measurements taken from the motor and the data that were inputted to Maxwell to build the model are covered as well as the assignment of appropriate material properties, starting with the preliminary data that was provided by the motor manufacturer and other companies, and moving on to the measurements made.

3.1 Preliminary motor data

It is common for buyers to receive some basic data about the motor they are buying, which are usually more than enough to operate the motor without needing to know the specifics. This data can, however, start lacking when the buyer is starting to model and simulate the motor in FEM (Finite Element Method) applications. For a simple parametric model, such as the ones used in Simulink, this data could just be enough to model the motor, but when using FEM, accurate geometries and material properties are required for it to produce reasonable results.

Preliminary data provided by the motor manufacturer in this case included the already mentioned rated and peak values for voltages, currents, torque and power. In addition to these, the team received parameters for winding losses and total losses, which are derived from stator iron losses and rotor losses added on to the winding losses. The team also received the torque constant, BEMF (Back Electromotive Force) constant, motor constant, phase resistance and inductance, maximum speed, number of pole pairs and the outer and inner diameters of the stator as well as its length. The team was also made aware that the windings are star connected.

The torque constant provides information on how much torque the motor produces per amps (rms) applied. The BEMF constant expresses the voltage (rms) induced per rotor speed in radians per second. The motor constant expresses how much torque the motor produces per input power squared in watts. In addition to these, the manufacturer provided the team with some performance curves for speed-torque, current-torque, speed-power and losses-speed. Unfortunately, from the data it was not clear if they were from simulations, testing or analytic calculations, as each method inherits some error i.e., the expected error between the data and the actual motor was uncertain. This is further elaborated in section 7.1.

3.2 Stator geometry

As stator geometry was not provided by the motor manufacturer, it remained unknown until the FEM simulations for the motors were started. During season 23, one of the team’s motors broke down and was retired. This allowed some reverse engineering to be conducted on the broken motor to uncover more information than was provided by the manufacturer. At this point, the motor was in a condition that can be seen in figure 5.

Figure 5. The teams broken motor used for reverse engineering.

As can be seen in figure 5, the stator is completely covered by a black resin-epoxy. This is very common with electric motors and there are a few reasons why this is done. Firstly, it is used to hold down the windings and stop them from moving in the stator slots. Secondly, it helps with heat dissipation as it replaces essentially all the air around the stator core and windings, as well as providing electrical and environmental insulation to them. Lastly, perhaps in a more of an add-on feature, it hides all the stator tooth and winding designs revealing little to the user about what is under the epoxy.

For FEM-simulation, it is necessary to know the geometry of the stator tooth and winding layout, so the epoxy had to be removed. There are a few methods available for this. Some epoxies can be dissolved with chemicals, but a more straightforward method is to use heat, which was used in this case.

Motor manufacturers typically do not make all parts of the motor themselves, but rather buy the materials and products which they use then to assemble the motor. In this case, the motor manufacturer had bought a resin-epoxy for the stator and, fortunately, they provided the team with their material datasheet. From this datasheet the team could get an idea of the temperature needed to remove the epoxy from the stator. Eventually, the stator was placed in an industrial oven at 200ºC for about 30 minutes, and after it was removed, the epoxy had softened enough, that it could be peeled off the stator. This required a few cycles as the process was very time-consuming and the epoxy cooled down and hardened again. With this method, most of the epoxy was removed successfully and a heat gun was used to get the last minor traces off. By the end of this process the winding layout and stator geometry could be seen. In figure 6, the motor with most of the epoxy removed can be seen.

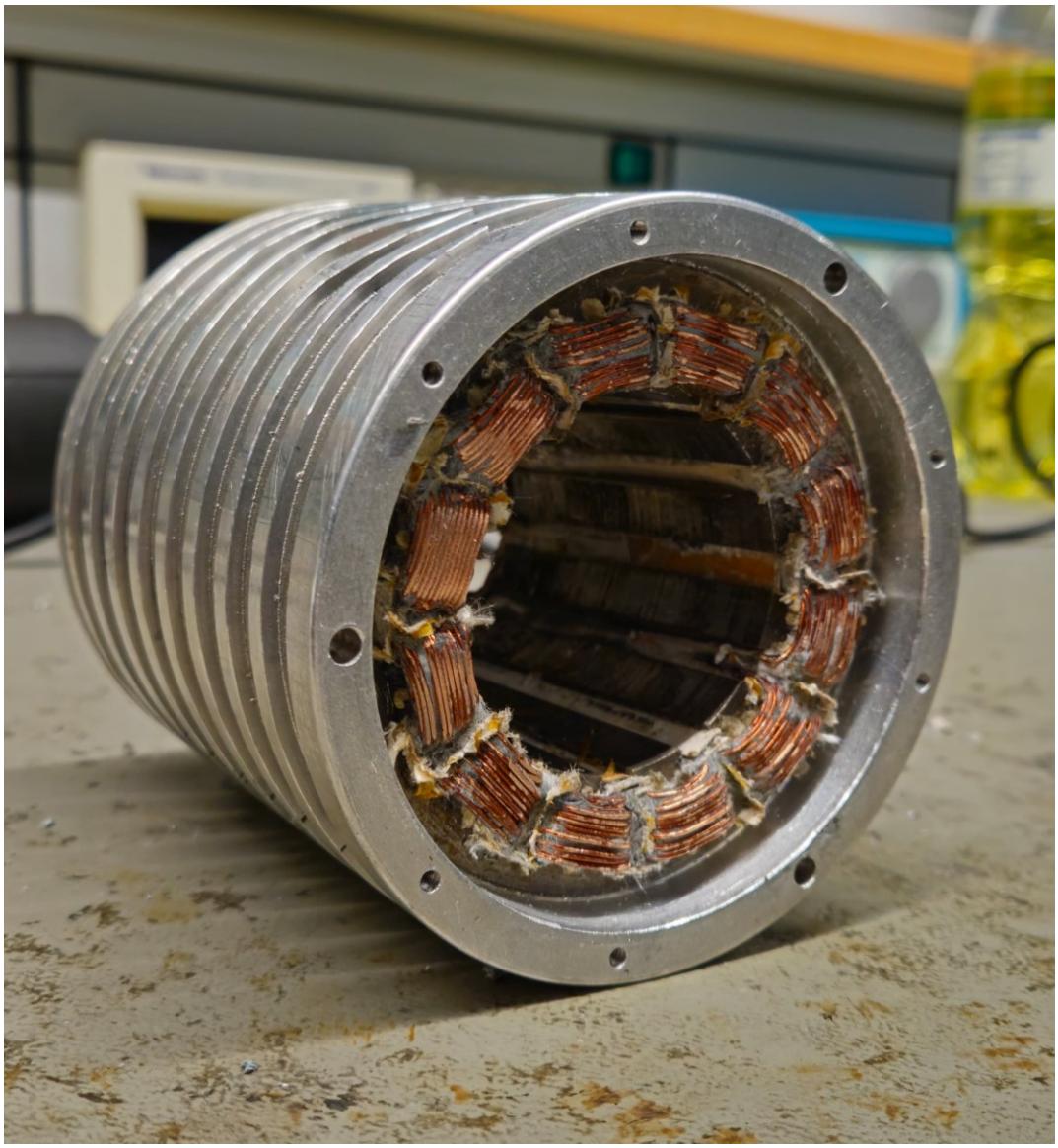

Figure 6. Team’s motor with most of epoxy removed.

Electric motors have laminated cores to eliminate eddy currents in the core material. This allowed the removal of a segment of a single sheet of the stator core steel, but it also required the removal of some of the windings around it. The removal was necessary for the measurement of slot geometry. From the data sheet provided, the inner and outer diameters were obtained, but for the slot dimensions they required measuring. There are several approaches for completing the measuring of slot geometry. The most precise methods would be using a high precision measuring probe or alternately a high precision 3D-scanner. For this project, these options were not available, but a profile

projector was used instead. The projector in case was a Mitutoyo model PJ311 profile projector. In figure 7, the measurement of the stator slot dimension can be seen.

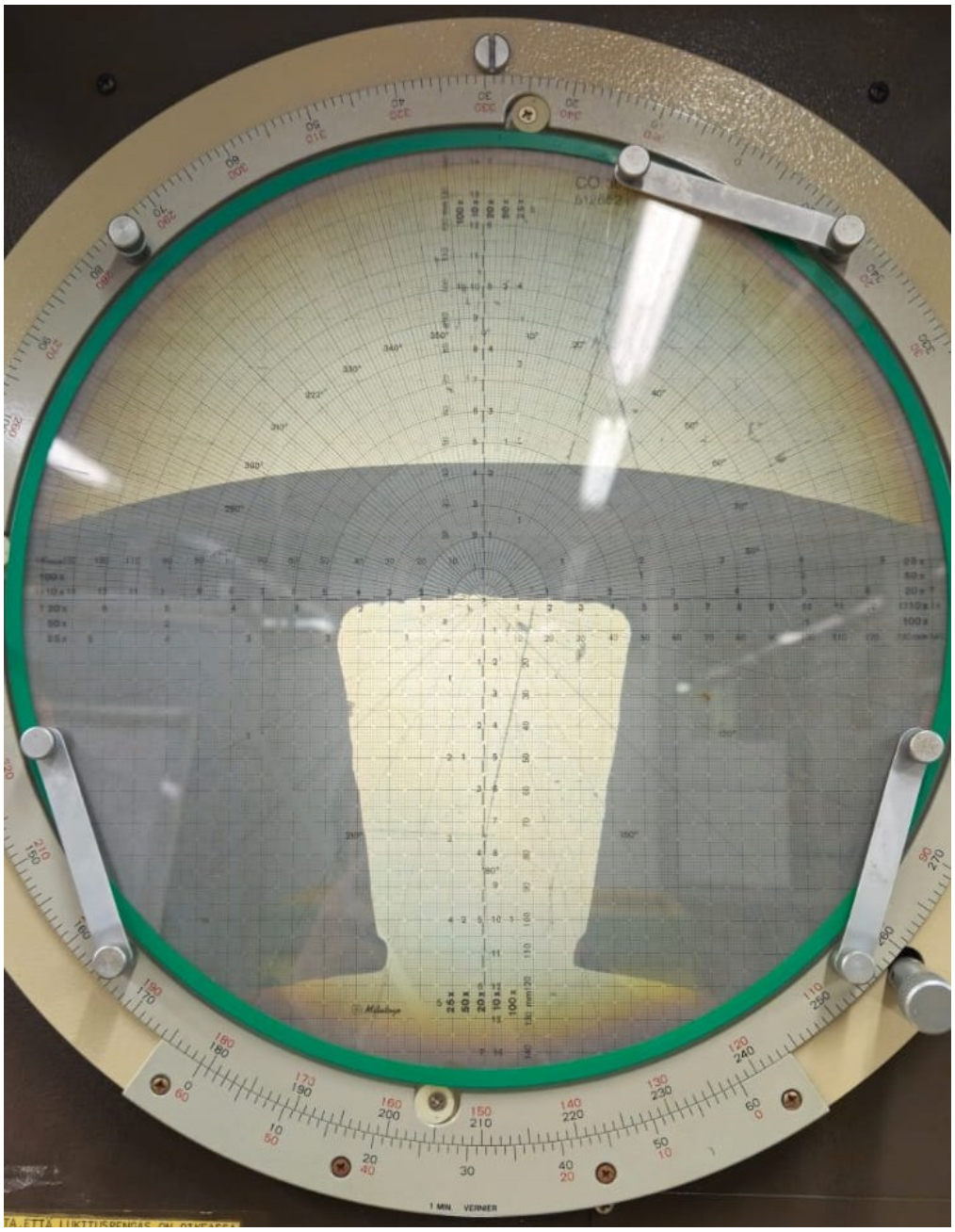

Figure 7. Stator slot measured with Mitutoyo profile projector.

As shown in the figure, the edges of the slot had some ripple, which was the aftermath of the removal unfortunately. However, a fairly accurate measurement was nevertheless obtained and used.

3.3 Winding layout

After the removal of the epoxy, the winding layout was examined. Visual examination revealed that the layout was a concentrated winding as none of the coils overlapped with each other and only circled one stator tooth. The slot count was also examined to be 12 and each phase having 4 coils in parallel separated evenly around the 12 slots. All the coils met at the end, coming to a neutral point creating the star connection. The turn count for each coil was measured to be 52.

The diameter of the copper wire was measured with a micrometre to be closest to AWG (American Wire Gauge) 22, which correlates to a diameter of 0,643 mm.

3.4 Material properties and material tester

For the core material the motor manufacturer provided a datasheet from the core material manufacturer as it was also outsourced. The data sheet included some information needed for the simulation, such as the stacking factor of the laminations. It also included the electric conductivity and other useful material properties. With some inquiry, the team was able to receive a B-H curve from the material manufacturer which can be considered necessary for the FEM-simulation. B-H curve represents how the material’s magnetic properties behave under magnetic loading with H being the applied external magnetic field and B the total magnetic flux density. The curve itself is shown in section 4. In addition to the B-H curve, a table for losses was also provided to calculate for core losses in the material. This is also presented in section 4.

It is rare for motor manufacturers to use two different core materials, one for the stator and another for the rotor. This can, however, be a possibility, so it should be verified. This was done with an Olympus Innov X Delta non-destructive XRF (X-ray Fluorescent) analyser. The results of the measurement indicated that they are the same material with very little discrepancies in the three most found elements which were Iron, Titanium and Manganese. Below in figure 8, the measurement process can be seen.

Figure 8. XRF-measurement of the core material.

A piece of the rotor lamination was removed for the measurement as well.

3.5 Magnetic properties

In the previous chapter, it was mentioned that the B-H curves were provided for the core material by the core manufacturer. The curve covers essentially all of the necessary magnetic properties besides for the permanent magnets. No preliminary information about the permanent magnets was provided by the motor manufacturer and as the strength of the magnet is very influential to the performance of the motor, some testing was required.

The magnets' elemental composition was also measured with the XRF-analyser. However, the measurement was somewhat inconclusive. The magnet had a nickel plating, indicating it being a neodymium magnet. Neodymium being one of the strongest magnetic materials available, makes it a very attractive choice for designers. Neodymium magnets are made of neodymium, iron and boron. Firstly, due to boron’s low atomic number, it is nearly invisible to XRF. Secondly, the measurement did not yield any value for neodymium. The analyser presents the material consumption as a percentage and its tolerance as well as a list of materials not detected. Unfortunately, neodymium was not on the list, suggesting that the particular analyser does not have the capability or the calibration for Neodymium measuring. There is no mention of the possibility of measuring neodymium on the user’s manual either. The magnet was shown to have an elemental composition having 80% iron and 7% manganese. (Olympus DS-2000 Specs 2010).

To estimate the strength of the magnet, a measurement of the flux density was necessary. The measurement was obtained with F.W. BELL hall effect gaussmeter model 5080 that can be seen in figure 9.

Figure 9. F.W. BELL Model 5080 Gaussmeter.

The measurement was attained approximately from the centre of the magnet as seen below in figure 10.

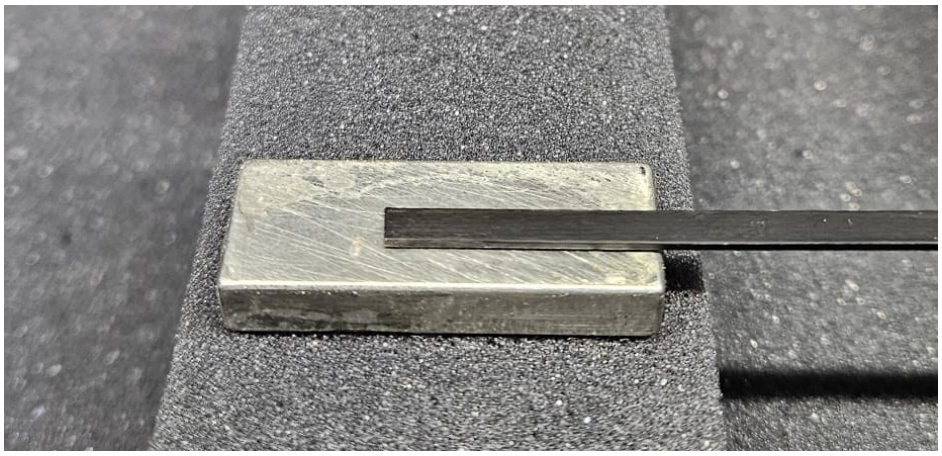

Figure 10. Permanent magnet flux density measurement.

This measurement was used to approximate the grade of the magnet as it was not mentioned in the preliminary data. For this, an online calculator was used, which approximates the grading by considering the magnets shape, side lengths and the flux density at a distance from the surface of the magnet in its axis of flux path. The calculation is for neodymium magnets and, all things considered, this was the most probable material.

Flux is often represented with lines going from a magnets north pole to the south pole. This is a simplified way of visualizing the phenomenon of magnetism. The lines itself represent the direction in which the magnetic domains of a material would align if placed in the magnetic field. The unit of flux is Weber (Wb), but when measuring a field, the flux density, which is the flux divided by the cross-sectional area, is used. One can picture a rounded tube with a source of flux on the other end. The flux density in the tube can be defined if the flux noted by Φ and cross-sectional area noted by A are known as seen in equation 1.

$$\boldsymbol{B} = \frac{\Phi}{A} \tag{1}$$

As result the flux density **B** as a vector quantity is produced and its unit is Tesla or equivalently Weber per square meter. (Hughes & Drury 2019.)

This was measured with the Gaussmeter or Teslameter. The naming indicates the units of measurement as it can be either one, as one Tesla equals 10 000 Gauss. The official measurement of magnetic materials is defined in IEC 60404-5 international standard. Essentially, to produce standard accurate results a VSM (Vibrating-Sample Magnetometer) is required (IEC 60404-5:2015). However, this was not available, and an educated guess based on the result of the gaussmeter had to be settled on. The formula used to calculate the flux density at a distance from the surface of the permanent magnet is seen in equation 2,

$$\boldsymbol{B} = \frac{B_r}{\pi} * \left(arctan\left(\frac{L*W}{2z\sqrt{4z^2+L^2+W^2}}\right) - arctan\left(\frac{L*W}{2(D+z)\sqrt{4(D+z)^2+L^2+W^2}}\right)\right) \quad (2)$$

where L, W and D are the side lengths of the magnet, Br is the residual magnetic field left after the removal of external magnetic field and z is the height at which the flux density is measured.

As the magnet was measured right on the surface, as was seen in figure 10, the only displacement represented by z was due to the sensor location inside the measuring probe. From the datasheet of the Gaussmeter, the sensor height was determent to be approximately 0,5 mm and this was used as the z value in the equation. The Gaussmeter gave a result of around 0,32 Teslas. Comparing the result to typical values of several N-rated magnets, the magnet in case was from the higher end of the ratings (42-52). (Camacho & Sosa 2013: 12.)

3.6 Skew angle

Skew angle can be used in electric motors to reduce cogging torque. It can be used either in the stator or rotor. It can be done in steps or continuously depending on whether the skewing element includes windings or magnets as well as the shape of the magnet. Usually, if square magnets are used, a stepped skew angle is chosen as the geometry makes it difficult to produce a continuous skew angle. In the case of windings, it is easy to use a continuous skew angle with the core material as the winding are relatively easy to bend to different shapes. The skew angle is achieved by rotating the core lamination material a set angle between lamination layers. Although it is rare, it is possible to achieve continuous skew angle with permanent magnets by using special curved magnets. In figure 11 on the left, permanent magnets skewed in steps can be seen and, on the right, coils in a continuous skew angle are shown (Krings & Monissen 2021: 4).

In the case of the team's motor, a continuous skew angle in the stator core was used. The rotor did not have any skew angle. The angle was measured using a

laser projector and an angle calibre. The measurement result was approximately 10 ±1 degrees.

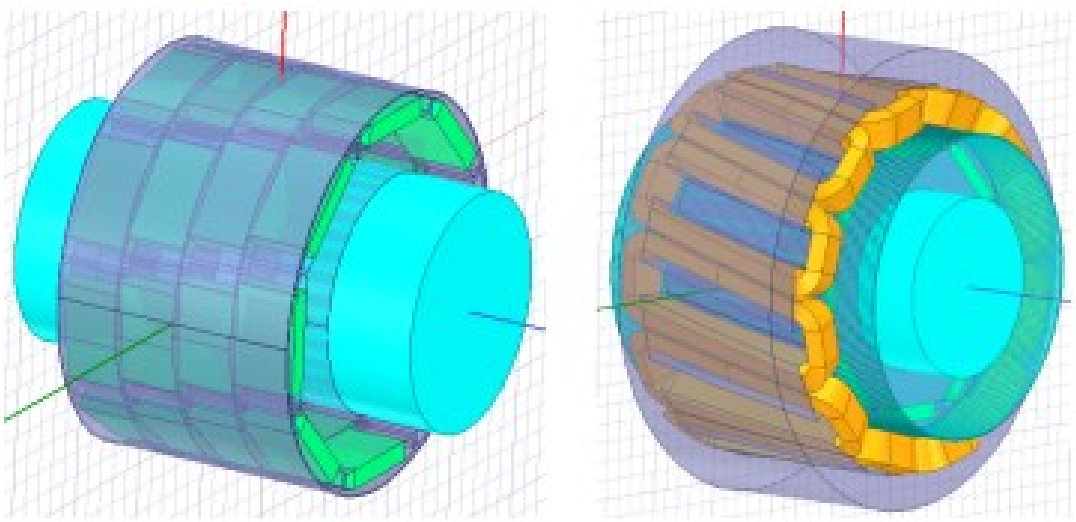

Figure 11. Examples of different types of skewing used in electric motors.

4 Modelling

In this chapter, the modelling process of the motor into Ansys Maxwell is covered. Majority of the details are listed with figures from RMxprt as they are in parametric forms. The majority of the modelling took place in Ansys RMxprt and with that, a Maxwell design was created.

4.1 Stator

With RMxprt, the motor type was chosen to be an IPM. This helps the software to narrow down the parameters needed to model the motor. Following this, the motor was set to be an inner rotor machine. The stator was set to the values found in figure 12.

	Name	Value	Unit	Evaluated Value	Description
	Number of Poles	8			Number of poles based on which the AC winding is wound
	Number of Slots	12			Number of slots of the iron core
	Circuit Type	S3			Drive circuit type
	Slot Type	4			Slot type of the iron core
	Position Control	☑			Drive circuit is controlled by position signals from position sensor

Figure 12. Initial stator set up in Ansys RMxprt.

In figure 12, the circuit type 3 refers to a star type winding connection, meaning that the ends of each coil meet at a neutral point. The slot type 4 refers to the general shape of the slot that can be seen below in figure 13.

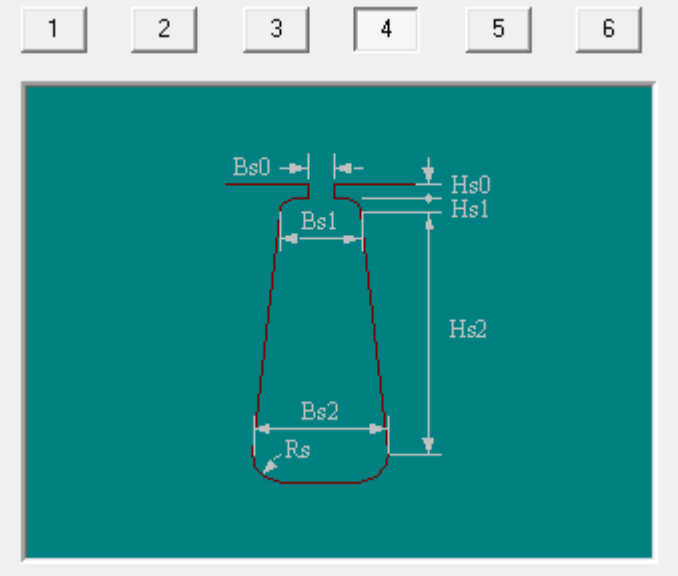

Figure 13. General slot shape of stator.

There are six general shapes of slots available in the RMxprt design where number four was the closest one in comparison to the actual stator slot that was seen in figure 7. The dimensions seen in figure 13 are used to define the slot geometry and the chosen values are listed below in figure 14.

	Name	Value	Unit	Evaluated Value	Description
	Auto Design	☐			Auto design Hs2, Bs1 and Bs2
	Parallel Tooth	☐			Design Bs1 and Bs2 based on Tooth Width
	Hs0	0.8	mm	0.8mm	Slot dimension: Hs0
	Hs1	0.2	mm	0.2mm	Slot dimension: Hs1
	Hs2	9.5	mm	9.5mm	Slot dimension: Hs2
	Bs0	5.8	mm	5.8mm	Slot dimension: Bs0
	Bs1	6.2	mm	6.2mm	Slot dimension: Bs1
	Bs2	9.2	mm	9.2mm	Slot dimension: Bs2
	Rs	1	mm	1mm	Slot dimension: Rs

Figure 14. Slot dimensions.

The rest of the stator core parameters can be seen in figure 15. The skew angle is seen to be 0 degrees, but this was only for the RMxprt model building and was changed afterwards in Maxwell.

	Name	Value	Unit
	Outer Diameter	85	mm
	Inner Diameter	51.6	mm
	Length	70	mm
	Stacking Factor	0.93	
	Steel Type	Electrical steel NO20-15	
	Press Board Thickness	0	mm
	Magnetic Press Board	☐	
	Skew Width	0	deg
	Lamination Sectors	0	

Figure 15. Stator dimensions and material information.

As was mentioned in chapter 3.4, the core material manufacturer did provide the team with a datasheet as well as the B-H curve. From the datasheet the stacking factor was set to be 0,93. As the core material is made of very thin steel laminations to reduce eddy currents, the amount of actual steel in the core is not 100%. Between each lamination, there is an insulation coating and, due to manufacturing tolerances, the surface is never completely flat. This is what

the stacking factor represents. It is the ratio of steel to insulation and air along the stacking direction of the lamination core. It is important to consider this, as the insulation and air have a very low permeability relation to the steel, which affects the simulation results. (Stacking Factor 2025.)

Maxwell considers the stacking factor by adjusting the B-H curves of the lamination material and reapplying the stator and rotor cores with a new adjusted material. This is done for B-H curves as well as B-P curves. (Maxwell Help 2024: 1284-1285.)

Maxwell offers a variety of default materials to use with the model, but as most of the used materials properties are known, a new material was created into Maxwell. This was possible with prebuilt tools inside of Maxwell allowing to create a new material. In figure 16, the material properties inputted to Maxwell can be seen.

	Name	Type	Value	Units
	Relative Permeability	Nonlinear	B-H Curve...	
	Bulk Conductivity	Simple	1930000	siemens/m
	Magnetic Coercivity	Vector		
	- Magnitude	Vector Mag	0	A_per_meter
	- X Component	Unit Vector	1	
	- Y Component	Unit Vector	0	
	- Z Component	Unit Vector	0	
	Core Loss Model		Electrical Steel	w/m^3
	- Kh	Simple	210.774100903013	
	- Kc	Simple	0.196029850662467	
	- Ke	Simple	0	
	- Y	Simple	1.97558675107058	
	- Kdc	Simple	0	
	- Equiv. Cut Depth	Simple	0.001	meter
	Mass Density	Simple	7650	kg/m^3
	Composition		Lamination	
	- Stacking Factor	Simple	0.93	
	- Stacking Direction		V(3)	
	Young's Modulus	Simple	0	N/m^2
	Poisson's Ratio	Simple	0	

Figure 16. Material properties of the core material.

From figure 16 the relevant values inputted were the bulk conductivity in siemens/m, the B-H curve, the core loss model, mass density and the composition data. The rest of the values were irrelevant for the electromagnetic simulation.

The relative permeability was inputted as a nonlinear type allowing for the use of the B-H curve provided by the core manufacturer. The curve itself can be seen in figure 17.

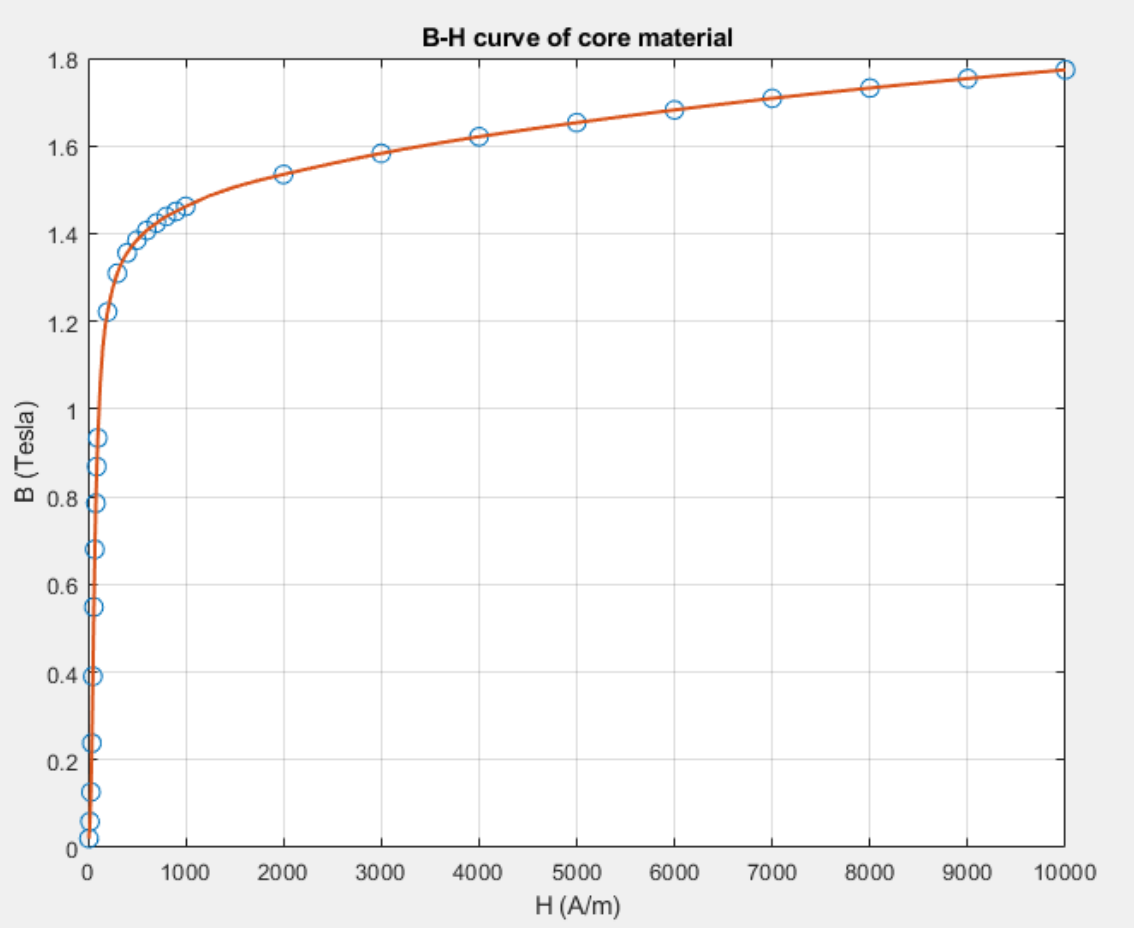

Figure 17. B-H curve of the core material.

The data was originally received as an .xlsx file, but it was converted to a .tab file for it to be imported into Maxwell. This was done with Matlab together with some interpolation as Maxwell gave a warning with the original dataset that there were gaps too large between data points.

Maxwell offers four different core loss models which are electrical steel, power ferrite, B-P curve and hysteresis model, which calculate the losses using different models. The core loss model was chosen to be an electrical steel, and the data was inputted as core loss versus frequency tables. For this, the datasets provided by the core material manufacturer were used, but they also had to be converted into .tab files in Matlab so that they could be imported into Maxwell. The data was inputted in total of 21 different data sets, each corresponding to the frequency at which the losses occur. Each data set has the B-P curve with B values from 0 to 1,5 Teslas and P values for the losses in Watts per kilogram. Below in figure 18, the core loss curves plotted in Maxwell can be seen. Each line represents a different frequency which vary from 50 Hz to 2000 Hz.

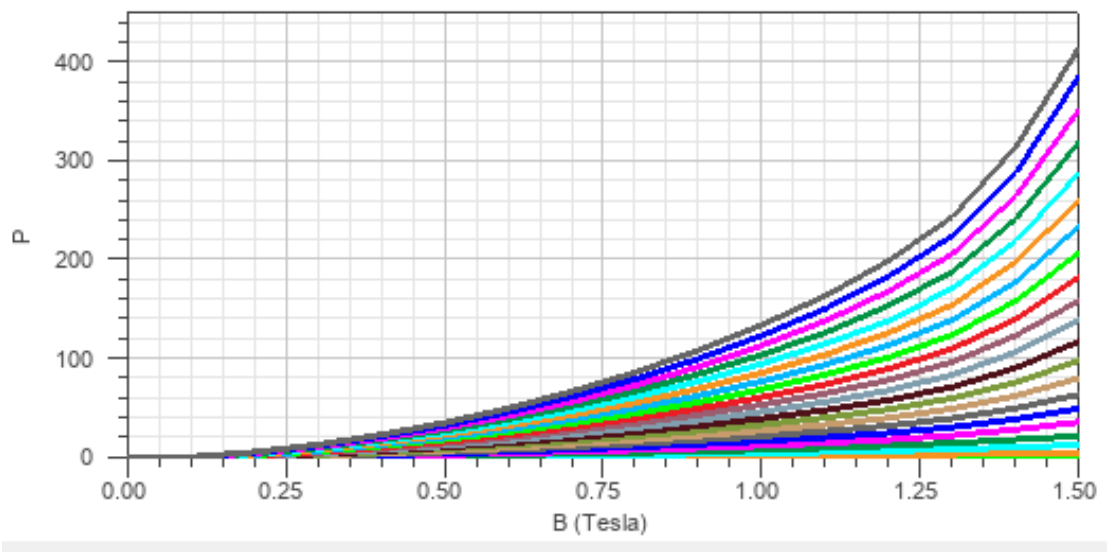

Figure 18. B-P curves of the core material.

In the case of the electrical steel core loss model, Maxwell uses Bertotti's loss model to calculate for the core losses. With the curves, it solves for the Bertotti loss coefficients. The equation of Bertotti's model used by Maxwell is seen below in equation 3,

$$P_{Fe} = K_h f B^Y + K_c f^2 B^2 + K_e f^{1,5} B^{1,5} \quad (3)$$

where f is the frequency, B is the amplitude of the applied sinusoidal flux density waveform and K_h, K_c and K_e are the Berrotti coefficients representing static hysteresis losses, dynamic eddy current losses and excess losses. The Y-term as the power of B for hysteresis core loss term was added later on as the model needed to be adjusted to new lamination materials. The Y term is derived from equation 4, where P_h is the total hysteresis loss.

$$P_h = K_h * f * B^Y \quad (4)$$

The eddy-current loss coefficient K_c is calculated as below in equation 5,

$$K_c = (\pi d)^2 * \sigma/6 \quad (5)$$

where d is the thickness of the lamination and σ is the conductivity of the material. The rest of the coefficients are derived by minimizing the error between measured and modelled curves as in equation 6,

$$err = \sum_{j=0}^{m-1} \sum_{i=0}^{n-1} \left(P_{mij} - P_{vij}\right)^2 = min \quad (6)$$

where P_{mij} is measured losses and P_{vij} are the modelled losses at different frequencies, m is the number of curves and n is the number of points on the measured core loss curve. (Maxwell Help 2024: 1298-1304.)

4.2 Rotor

The rotor modelling was started with general dimensions similar to the stator. Firstly, the number of poles for the rotor was inputted as 8. Then, the geometry was determined with length, inner and outer diameters and pole type as well as the material information. The values can be seen in figure 19.

	Name	Value	Unit	Evaluated Value	Description
	Outer Diameter	50.2	mm	50.2mm	Outer diameter of the iron core
	Inner Diameter	20	mm	20mm	Inner diameter of iron core
	Length	70	mm	70mm	Length of the iron core
	Stacking Factor	0.93			Stacking factor of the iron core
	Steel Type	Electrical steel NO20-15			Steel type of the iron core
	Pole Type	1			Pole type of the rotor

Figure 19. Rotor dimensions and material properties.

The length and the rotor inner diameter were provided in the motor datasheet. The outer diameter was measured with a calliper and a micrometre. The result showed an air-gap of 0,7 mm. The air-gap of an electric motor draws a lot of attention from the designer's point of view as it has the most reluctance. Reluctance is essentially the equivalent of what resistance is in electric circuits. In a magnetic circuit, reluctance in a way opposes the completion of the magnetic circuit, hence why it is wise to keep the air gap as small as possible. Of course, some clearance is unavoidable in order for there to be rotating movement. It can be seen how the reluctance plays a part in flux formulation in equation 7,

$$\Phi = \frac{NI}{R} \tag{7}$$

where N is the number of turns, I is the current in the conductor and R is the reluctance in H^-1. The upper part of the equation is known as the magnetomotive force (MMF) created by a coil and its unit is Ampere-turns. (Hughes & Drury 2019.)

In comparison to air, steel has a very low reluctance even though motors have significantly more steel than air in the magnetic circuit. This property allows the manipulation of where the flux flows, as it tends to stay inside the motor core material rather than leak to the outside air. There are limits to this, though, as the reluctance of the material is non-linear, as can be seen in the B-H curve. As the applied external magnetic field is increased, the rise of the total flux density begins to level out. When the material is no longer able to increase the flux

density, it is said to be saturated i.e., all of its magnetic domains have aligned. For steels, the typical value when the material will saturate is approximately 2 Teslas. Thus, designers aim to keep the material below the saturation level by dimensioning the iron parts so that the cross-section is large enough to carry the necessary flux without saturating. (Hughes & Drury 2019.)

From figure 19 above, it could be seen that the pole type was chosen at this point. As was mentioned above, the motor was a spoke type, so this was chosen. RMxprt offers six different types of pole types with two popular V-type design where the magnets are in a V-shape and square type, as well as a mixture of the two.

RMxprt then required the magnet dimensions, as shown in figure 20.

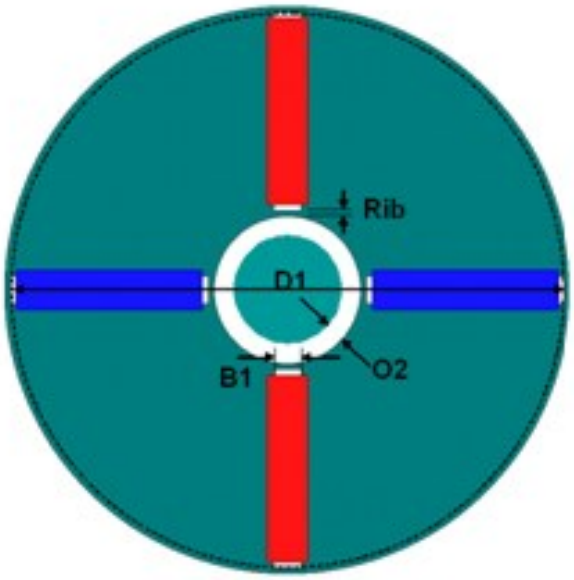

Figure 20. Magnet dimensioning.

The rotor is made of three essential parts. The core, the magnets and the shaft. With the spoke type rotor, leakage flux into the shaft should be avoided as it does not contribute to the torque production, which is why the shaft is often made of a nonmagnetic material with high reluctance. In the case of this

particular motor, it was manufactured from grade 5 titanium. The core material is inserted around the shaft with the magnets embedded into it. Some motors do inherent magnet ducts larger than the magnets itself to concentrate the flux, but in the team's motor, the ducts were of a similar size as the magnet. The dimension of the magnets and the ducts can be seen in figure 21.

	Name	Value	Unit	Evaluated Value	Description
	D1	48.5	mm	48.5mm	Limited Diameter for magnet ducts
	O2	0	mm	0mm	Magnet duct dimension:O2
	B1	6	mm	6mm	Magnet duct dimension:B1
	Rib	0.01	mm	0.01mm	Magnet duct dimension: Rib
	Layers	0		0	Number of duct layers
	Layer Pitch	0	mm	0mm	Pitch between two duct layers
	Magnet Thick...	6	mm	6mm	Magnet thickness, or duct thickness
	Magnet Width	14	mm	14mm	Total width of all magnets per pole
	Magnet Type	NdFe30			Magnet type

Figure 21. Magnet and magnet duct dimensions.

The rib dimension of 0,01 mm was inputted as RMxprt does not allow a rib length of 0. Initially, the magnet material was chosen to be NdFe30 from Ansys material library. It would be ideal to input the B-H curves for the magnet as well, but, as mentioned earlier, little to no information was provided about the magnets. The only value inputted for the magnet was the evaluated residual flux density of about 1,3 T. Other magnets from Ansys material library were tested with the simulations, and the one that produced the closest results was chosen for the final solutions. Material for the shaft was chosen to be titanium from the material library.

4.3 Windings

The goal of a 3-phase winding is to produce the stator rotating MMF that links with the rotor MMF to produce torque. The windings of the motor were introduced earlier to be a concentrated winding with 52 turns per coil in 12 slots. Concentrated winding is one of the two most popular ways of winding an

electric motor. The other option is a distributed winding. The difference lies in how many teeth the individual coils are wound upon. In a concentrated winding this is always one, but in a distributed winding, it is a minimum of two but can be more. With a concentrated winding, the length of the motor can be a little smaller, because in a distributed winding many of the coils have to be stacked on top of each other requiring more length in the motor ends. Concentrated windings experience a more of a trapezoidal electromotive force (EMF) waveform or sometimes known as the back-EMF resulting in high torque with comparison to distributed winding. Due to this, the concentrated winding does inherent more harmonics causing it to have more losses at higher speeds. In addition, the torque ripple is higher with concentrated windings.

EMF is essentially the applied force to a current carrying conductor that is moving relative to a magnetic field. The force itself is a product of the flux density, the velocity of the conductor relative to the field, and the length of the conductor. Usually, the result is presented as the voltage induced inside the conductor. This voltage, when motoring, is in the opposing direction to the applied voltage of the conductor. This is why field weaking is required in order to achieve higher speeds, as the velocity increases so does the EMF and the opposing voltage. By weakening the field, the flux density is reduced and as a result, less voltage is induced. Essentially, if the EMF is lower than the applied voltage, current will be positive and the motor will experience motoring torque and if the EMF is higher than the applied voltage then the current is negative and the motor is regenerating i.e., turning mechanical energy to electrical energy. (Hughes & Drury 2019.)

The inputted winding parameters can be seen in figure 22.

	Name	Value	Unit	Evaluated Value	Description
	Winding Layers	2			Number of winding layers
	Winding Type	Whole-Coiled			Stator winding type
	Parallel Branch...	1			Number of parallel branches of stator winding
	Conductors pe...	104		104	Number of conductors per slot, 0 for auto-design
	Coil Pitch	1			Coil pitch measured in number of slots
	Number of Stra...	1		1	Number of strands (number of wires per conductor), 0 for auto-design
	Wire Wrap	0	mm		Double-side wire wrap thickness, 0 for auto-pickup in the wire library
	Wire Size	Diameter: 0.643mm			Wire size, 0 for auto-design
	Conductor Type	copper			Steel type of the stator core

Figure 22. Winding parameters.

The winding is 2-layer, indicating that each slot shares the space with two individual coils. The coil pitch of a concentrated winding is essentially the same as the slot pitch. The conductors per slot was inputted as 104, as each coil had 52 turns and each slot had two coils. The number of strands, meaning the number of wires within a conductor, was one and the wire diameter was chosen from the wire library to be 0.643 mm or AWG 22. The conductor material was chosen to be copper from the material library and no specific information on it was altered.

With the presented topology, the slots per pole per phase or s/p/p is 0,5 and as mentioned earlier the windings are star connected. The star connection refers to the way the phases connect to each other. The two basic layouts are star and delta which can be seen in figure 23.

Figure 23. Star (left) and delta (right) connection of a 3-phase winding.

The differences lie within the voltages and currents in the phases depending which connection is used. In the star connection, the line voltage is root three

times the phase voltage, whereas in delta, line voltage and phase voltage are the same. Line current in the star connection is the same as the phase current and root three times phase current for delta connection. (Ravi 2024.)

The final winding layout can be seen in figure 24.

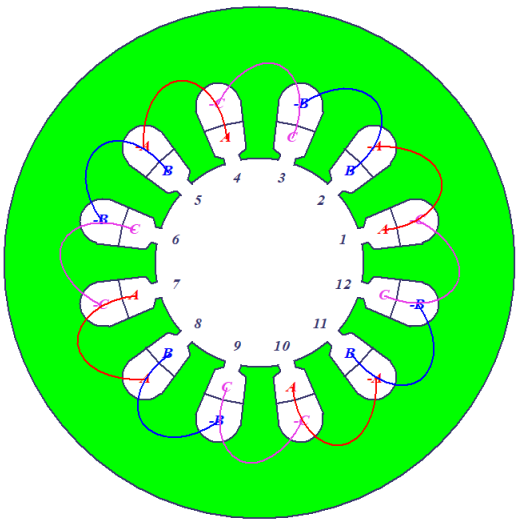

	Phase	Turns	In Slot	Out Slot
Coil_1	A	52	1T	2B
Coil_2	B	52	2T	3B
Coil_3	C	52	3T	4B
Coil_4	A	52	4T	5B
Coil_5	B	52	5T	6B
Coil_6	C	52	6T	7B
Coil_7	A	52	7T	8B
Coil_8	B	52	8T	9B
Coil_9	C	52	9T	10B
Coil_10	A	52	10T	11B
Coil_11	B	52	11T	12B
Coil_12	C	52	12T	1B

Figure 24. Winding layout inputted to RMxprt.

In figure 24, one of the coils seem to be on the inner edge and the other on outer edge of the slot, but this is not correct as figures 4 and 6 more accurately show that the coils are side by side in the slots. This is characteristic to the RMxprt visualisation of the winding layout and does not affect the actual model.

5 Simulation setup

In this chapter, the simulation setup is covered after the creation of the motor model was complete. The order in which the setup is completed is not important and decided by the user.

5.1 Mesh

FEM calculations typically involve dividing a problem into smaller elements, where forces are computed for each element. This approach enables the analysis of geometries that would otherwise be too complex to calculate directly. Mesh is the collection of these elements. With Maxwell, the mesh can be automatically or manually created. It can be difficult to know exactly how many elements are needed for accurate results and the only way to go about it is by running the calculation with mesh refinements and observing the results (Gieras 2010: 103-104). By the time the rate of change in result has decreased to some decimals, it is usually dense enough. Further increasing the element count would result in unnecessary increase in computing power and time.

In electromagnetic problems, and especially with Ansys, the software uses FEM to calculate for Maxwell's equations. The first of which is seen in equation 8,

$$\nabla * \boldsymbol{H} = \boldsymbol{J} + \frac{\partial \boldsymbol{D}}{\partial t} \tag{8}$$

where **H** is the vector magnetic field intensity, **J** is the vector electric current density and ∂**D**/∂t is the density of displacement current where **D** is the vector electric flux density. The second equation is seen in equation 9,

$$\nabla * \boldsymbol{E} = -\frac{\partial \boldsymbol{B}}{\partial t} \tag{9}$$

where **E** is the vector electric field intensity and **B** is the vector magnetic flux density. The third equation is seen in equation 10,

$$\nabla * \boldsymbol{D} = \rho v \tag{10}$$

where ρv is the volume charge density. The 4th Maxwell's equation is seen in equation 11,

$$\nabla * \boldsymbol{B} = 0 \tag{11}$$

which indicates that there are no magnetic charges. All the four equations are presented here in differential form, hence the use of nabla, which is a vector operator that has no physical meaning or vector direction. The bolding of the letters is an indication of a vector quantity. (Gieras 2010: 93-95.)

The produced mesh for the motor can be seen in figure 25.

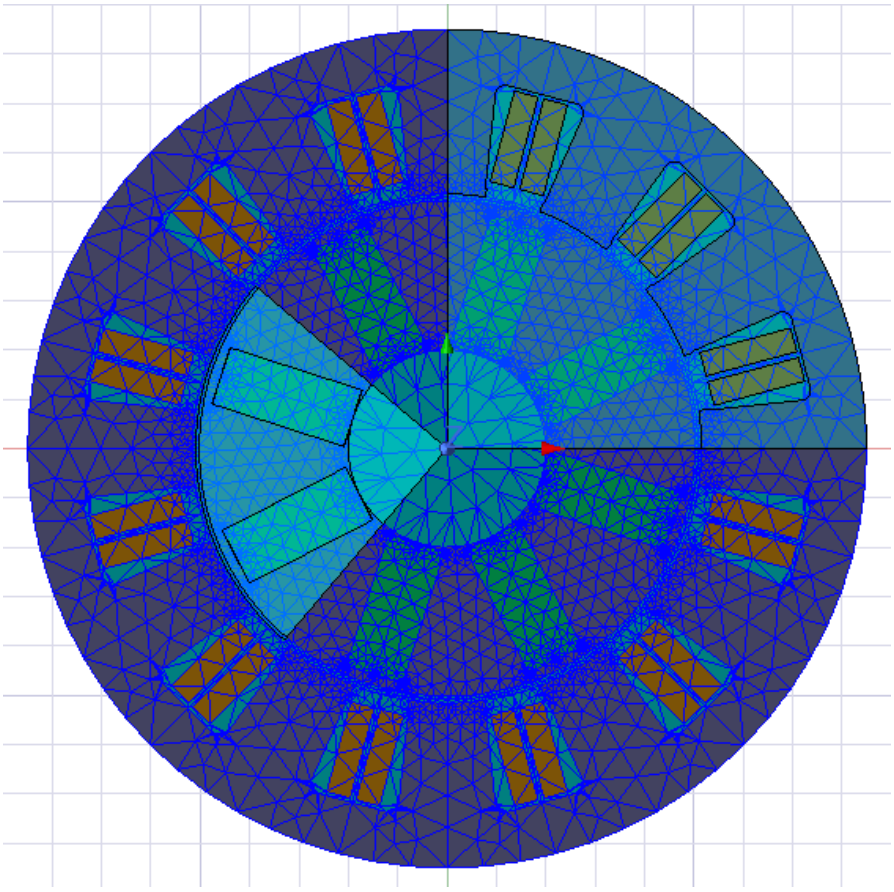

Figure 25. Automatically produced initial mesh.

The mesh in figure 25 is the initial mesh of the model, as for the final calculations Maxwell does adaptive meshing based on the reported error in the solutions, which is only available with static solvers. For transient solutions, the initial mesh is the final mesh. The number of elements created can be controlled separately by placing a maximum or a minimum.

After the generation of mesh either manually or by running the analyses, the mesh statistics can be observed. From there, it can be seen that for this case a total number of 2310 elements were created, and the division can be seen in figure 26.

	Num Elements	Min edge length	Max edge length	RMS edge length	Min elem area	Max elem area	Mean elem area	Std Devn (area)
Band	96	0.00035	0.000898074	0.000648498	1.43719e-07	1.45723e-07	1.44721e-07	1.00202e-09
Coil_0	11	0.000866846	0.00396117	0.0022905	4.67382e-07	4.89907e-06	2.13638e-06	1.50905e-06
Coil_1	11	0.000866846	0.00396117	0.0022905	4.67382e-07	4.89907e-06	2.13638e-06	1.50905e-06
Coil_2	11	0.000866846	0.00396117	0.0022905	4.67382e-07	4.89907e-06	2.13638e-06	1.50905e-06
CoilRe_0	11	0.000866846	0.00396117	0.00230656	4.67382e-07	4.89907e-06	2.13638e-06	1.50905e-06
CoilRe_1	11	0.000866846	0.00396117	0.00230656	4.67382e-07	4.89907e-06	2.13638e-06	1.50905e-06
CoilRe_2	11	0.000866846	0.00396117	0.00230656	4.67382e-07	4.89907e-06	2.13638e-06	1.50905e-06
InnerRegion	124	2.68587e-05	0.00104637	0.000358118	4.6965e-10	1.40475e-08	5.19847e-09	4.24304e-09
Mag1_0	222	3.49718e-05	0.0030099	0.00100263	9.81984e-10	2.79623e-06	3.78378e-07	5.75501e-07
Mag1_1	222	3.49718e-05	0.0030099	0.00100263	9.81984e-10	2.79623e-06	3.78378e-07	5.75501e-07
OuterRegion	372	0.000103528	0.00396117	0.0012497	5.57906e-09	3.59923e-06	3.61663e-07	5.55466e-07
Rotor	680	1e-05	0.00254855	0.0009602	6.31234e-10	2.05694e-06	3.64353e-07	5.70917e-07
Shaft	24	0.00130806	0.00395656	0.0033736	2.17544e-06	4.57571e-06	3.26315e-06	1.07393e-06
Stator	504	0.000103528	0.0053635	0.00178416	1.92942e-08	7.81263e-06	1.2553e-06	1.72532e-06

Figure 26. Mesh statistics.

5.2 Circuit and excitations

In Maxwell, the excitation of windings can be done in three ways, where the most accurate one is to use an eternal circuit, and the simple way is to use Maxwell's built-in excitation. The simple way is to create the phases and add windings corresponding to each one. By assigning each coil to their corresponding winding, their excitation is determined by the input of the phase. The input to the phase can be either voltage or current.

For this simulation, the current source was chosen as the manufacturer had stated nominal values for currents at different duty types. The current source is applied as a sine equation to the phases to produce the rotating magnetic field. The equations for phase A, B and C are presented in chapter 6.2. A voltage source for comparison can be issued for phase A, B and C as shown in equations 12, 13 and 14,

$$V_A = V_p * \sin(2\pi * f * t) \tag{12}$$

$$V_B = V_p * \sin\left(2\pi * f * t - \frac{2\pi}{3}\right) \quad (13)$$

$$V_C = V_p * \sin\left(2\pi * f * t - \frac{4\pi}{3}\right) \quad (14)$$

where V_A, V_B and V_C are the phase voltages, V_p is the peak phase voltage, f is the source frequency, and t is the time. The voltage waveform is inputted in radians, hence the use of π factors and not angles. The minus parts in equation 13 and 14 are equivalent of -120º and -240º, creating the phase lag.

The other more accurate method is to use an external circuit. With external circuit it is possible to model, for example, the inverters. This creates a more realistic excitation, as it can include power switches, diodes and the battery, as well as the control circuit of the power switches. It allows the user to control the switches with DC, AC or PWM sources. An example of this type of external circuit used in another project can be seen in figure 27.

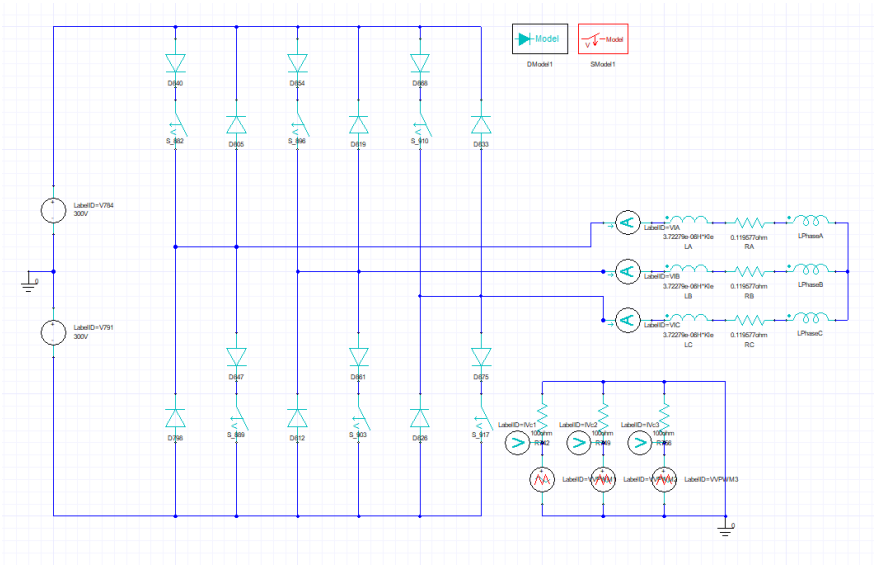

Figure 27. Maxwell external circuit.

5.3 Symmetry

Symmetry is one of, if not the most, useful aspect to leverage when running a finite element analysis (FEA). Symmetry is widely used in mechanical systems,

fluid dynamics, and many other applications of FEA because it reduces computational effort, leading to faster calculations and lower power consumption. As FEA is based on the calculation of forces for the elements, cutting the model in half directly removes half of the elements. This is possible when there is a force that acts evenly on an object that inherits an axis of symmetry. In case of the motor, it can be divided into four fractions, leaving the solver only one quarter of the motor to calculate the forces for. The rotor could have been divided into eight fractions, as there are eight poles in it. The magnetic field created by each pole is essentially the same, ignoring minor differences in material quality. However, the winding layout makes the use of eight fractions impossible. To properly excite the windings, they must be physically in the model and the minimal fraction of the motor that includes all three phases is one quarter. Axial symmetry is also possible and just as useful when doing 3D simulation. Maxwell post-processes the result by multiplying them with the number of fractions used to yield the results corresponding to a full model.

5.4 Boundaries

Ansys Maxwell does not essentially require the typical physical restraints as boundary conditions that a mechanical simulation would, because electromagnetic fields do not have any natural boundaries. There is no need to fix the stator or restrict the movement of rotor. The rotor rotation is simply assigned to an axis, and it is provided with initial position and velocity. The initial position is necessary for the rotor’s direct axis to be aligned with phase A at the start. The rest of the boundaries are there to simplify the problem.

There are, however, some electromagnetic specific boundaries required. One of the essential ones is the vacuum around the motor. In reality, the motor is surrounded by other components and air, but for the sake of the simulation, all the surroundings and the air gap are considered to be a vacuum.

There is also a vector potential boundary applied on the outer edge of the stator limiting all magnetic flux on the edge to 0. This is done to avoid leakage flux computation on the outer medium. It is called a Dirichlet boundary condition, as by the definition, it requires the magnetic vector potential to assume a prescribed value. This is a reasonable simplification as most of the flux would remain in the core material. (Gieras 2010: 102.)

Due to the applied symmetry condition, the symmetry axis must have boundaries as well. This is done by assigning the x-axis an independent boundary and the y-axis a dependent boundary. The boundary forces the dependent surface to inversely match the magnetic field of the independent surface at each corresponding point. (Maxwell Help 2024: 3687.)

6 Post-processing

6.1 Field overlays

From the magnetostatic simulation, the flux density in the core material due to the magnets can be seen in figure 28.

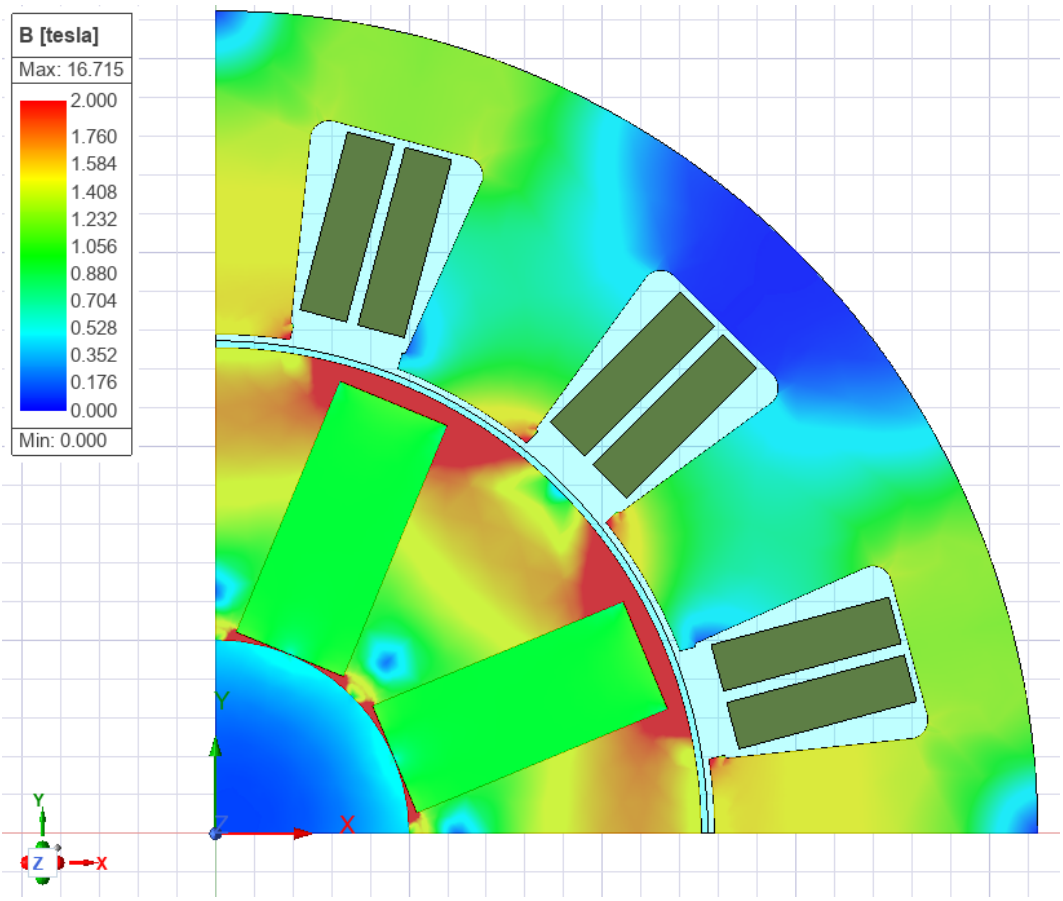

Figure 28. Flux densities caused by permanent magnets.

As can be seen in figure 28, the rotor outer regions by the permanent magnets are heavily saturated, but the stator tooth remains fairly well below saturation limits.

In figure 29, the flux lines passing through each component can be seen.

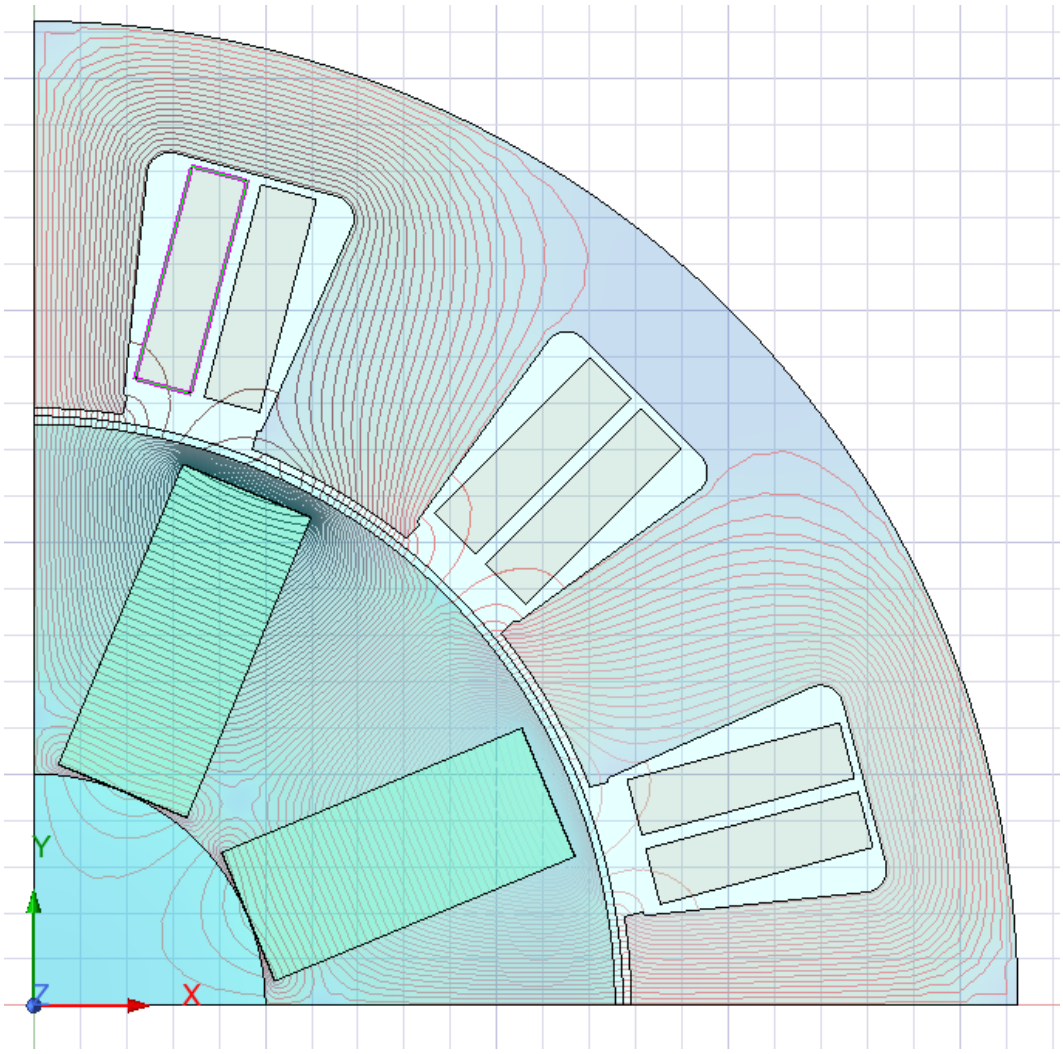

Figure 29. Flux lines of permanent magnets field.

As was mentioned in the introduction, the magnets are circumferentially excited, which can be seen in figure 29 with the lines representing the direction of flux. It can also be noted that some of the flux is circling inside the shaft which is an unwanted feature as it does not contribute to torque production. Figure 29 also visualises the vector potential boundary on the outer edge of the stator. Below in figure 30, the flux lines created by the permanent magnets for the entire motor can be seen.

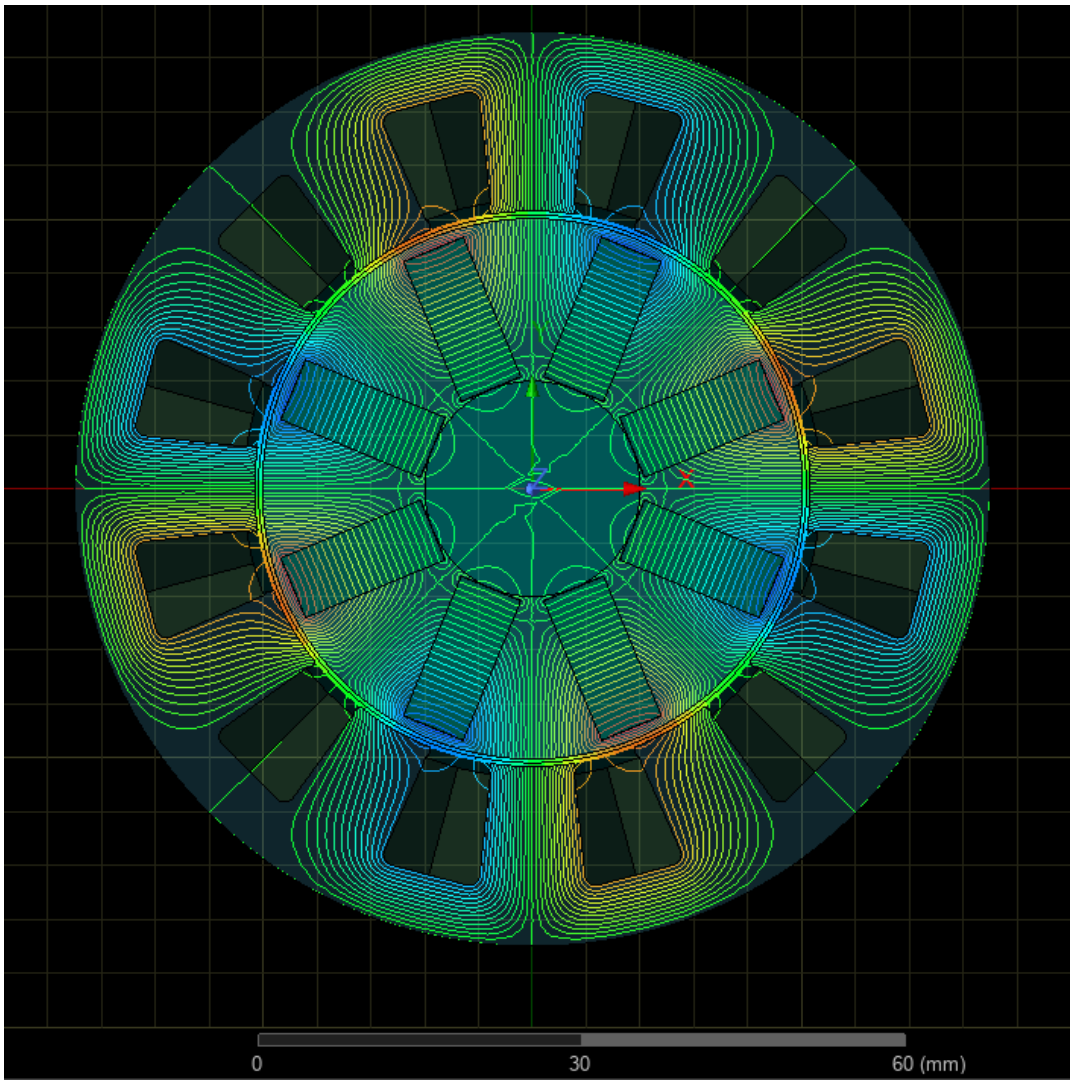

Figure 30. Magnetic field created by permanent magnets.

With the magnetostatic simulation, the leakage flux factor can be computed. The result was approximately 0,7, which is relatively low. The leakage factor indicates how much of the flux passing through the magnet is also passing through the air gap. Essentially signifying the ratio of all flux to useful flux. Its calculation is seen in equation 15,

$$K_L = \frac{\Phi_p}{\Phi_m} \tag{15}$$

where Φp is the pole flux and Φm is the magnet flux. Maxwell does not have the leakage factor as a default output variable, but it can be derived using the

software's built-in calculator. Note that in some literature the leakage factor is defined as the total flux produced divided by the useful flux resulting in a value over 1.

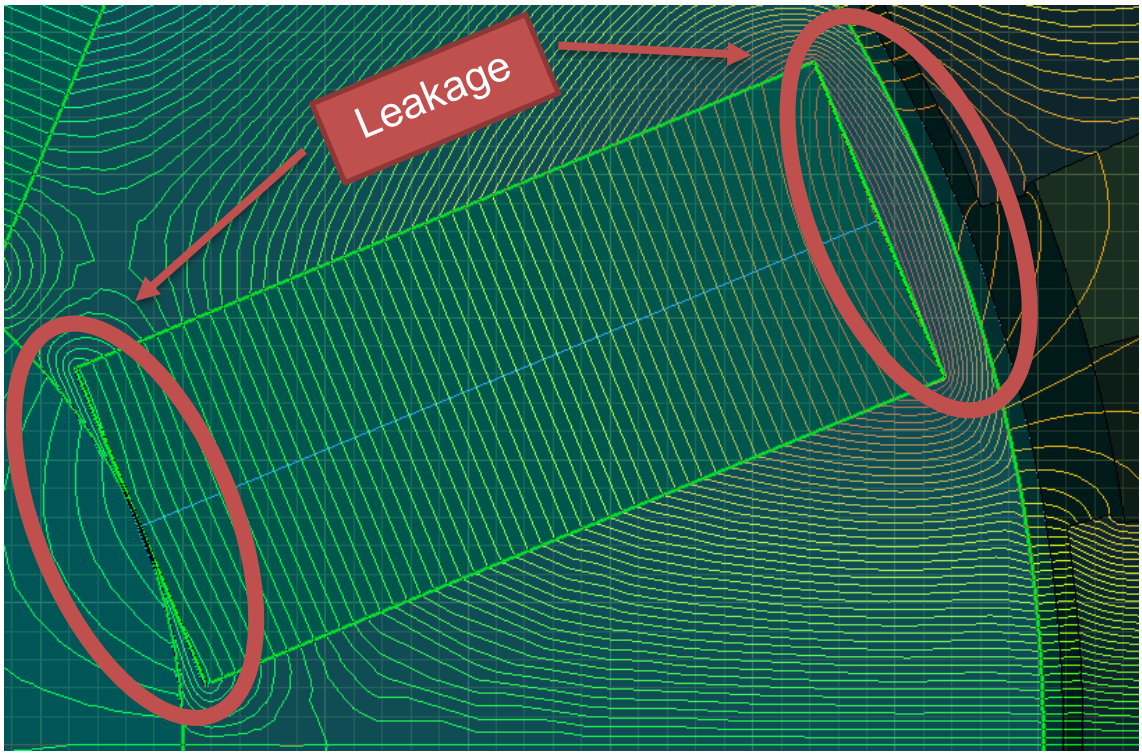

Figure 31. Flux plot of 1 magnet.

In figure 31, a closer look at the flux lines is seen. The leaking flux lines are circled with large red ovals. With a spoke type rotor, the leakage in the shaft side is almost inevitable, but fairly small, because of the weak magnetic properties of the shaft. On the outer edge, however, the flux has a very good path in terms of material properties, because it is going through the yoke of the rotor. This can be managed by dimensioning the yoke as small as possible, but a mechanical integrity standpoint is to be considered. So, in conclusion, it can be difficult, especially with a high-speed motor, to remove all the leakage flux in the rotor yoke, but it can be managed.

It is worth mentioning how geometry sensitive the leakage flux is. As the minimum distance from the edge of the magnet to the edge of the rotor core was measured by a hand calibre, there is most likely some error in the

measurement in the tenths/hundreds of mm. To know precisely the placement of the magnet, a high precision measurement tool would be required, but for this simulation the calibre and the profile projector provided a useful approximation.

As an experiment, the yoke width was altered to half the original size with a larger magnet duct, which resulted in the leakage factor rising to 0,8. However, the measurement made with the calibre and the profile projector was deemed accurate and the original values were used for the final model.

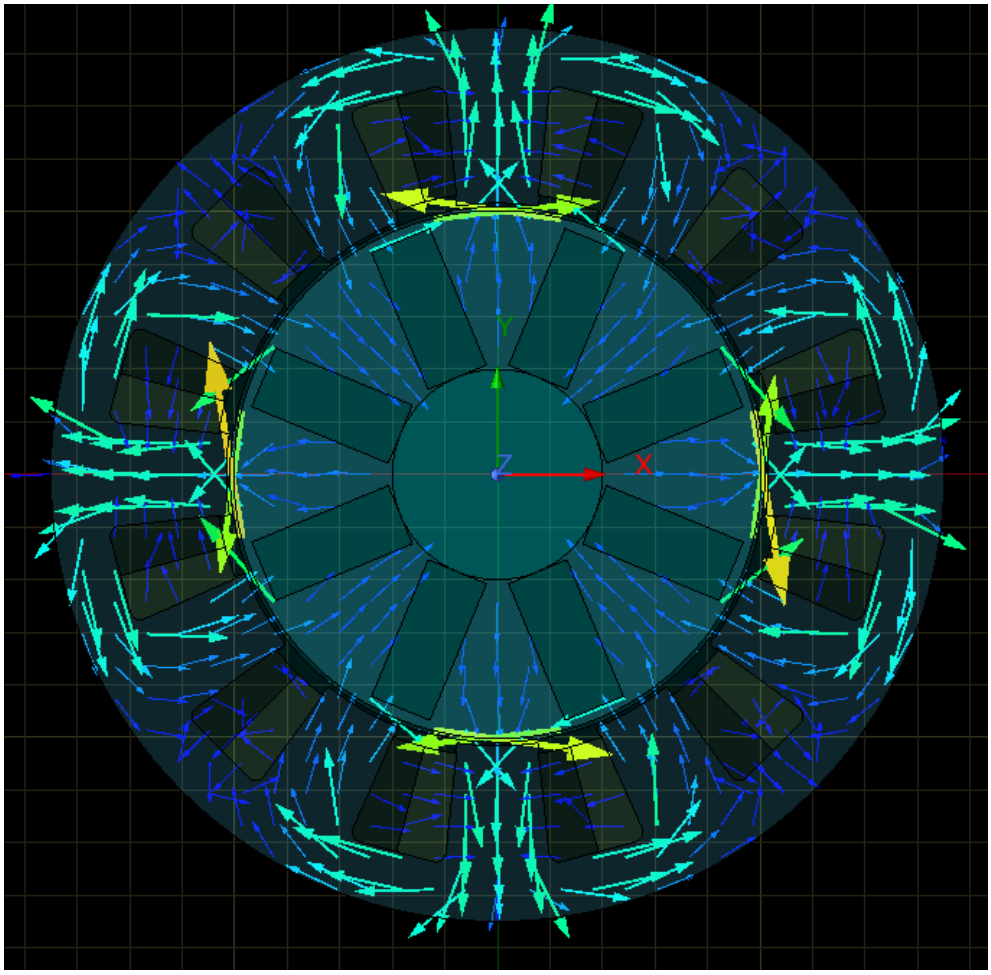

Figure 32. Magnetic field created by armature (magnets removed).

In figure 32, the field created by the armature is seen. The setup is further explained in chapter 6.2.

6.2 Plots

In figure 33, the winding flux linkage is plotted. The maximum value was approximately 56 mWb. This was simulated with a transient setup with the rotor having an angular velocity of 13250 rpm and no excitation in the armature.

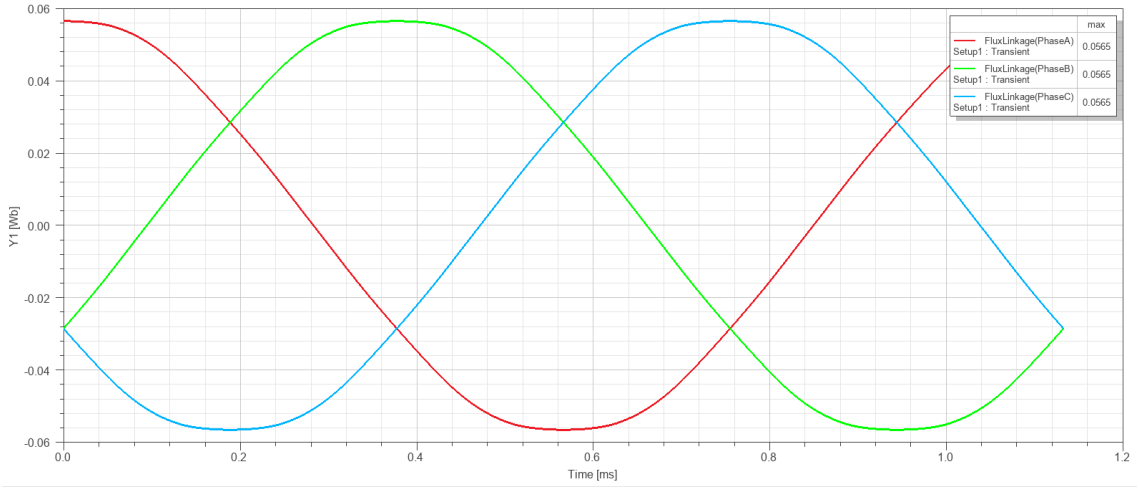

Figure 33. Winding flux linkage.

In figure 34, the cogging torque of the motor without a skew angle is plotted. The peak-to-peak value was approximately 2,7 Nm.

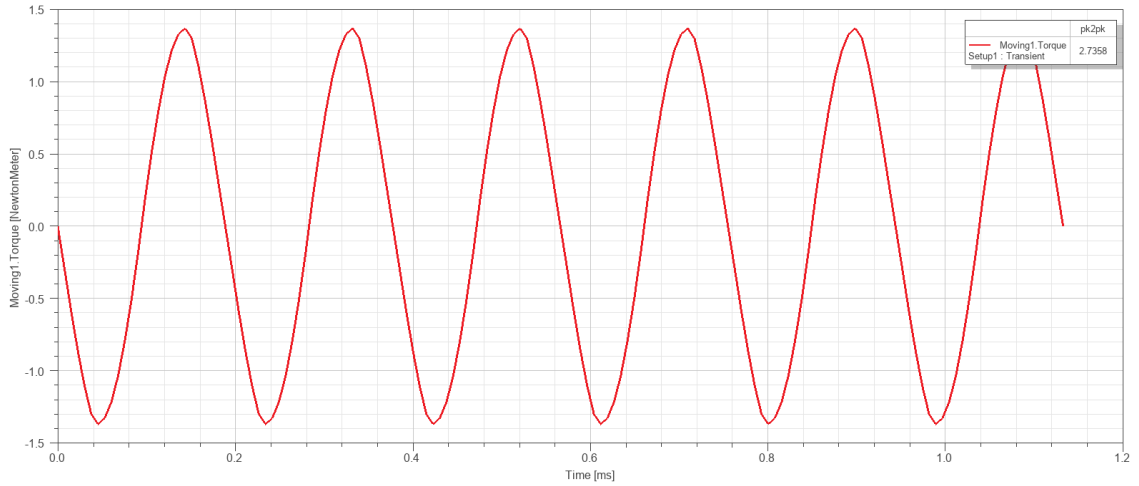

Figure 34. Cogging torque.

With the addition of the 10 degrees skew angle, the cogging torque reduced to approximately 1,2 Nm as seen in figure 35.

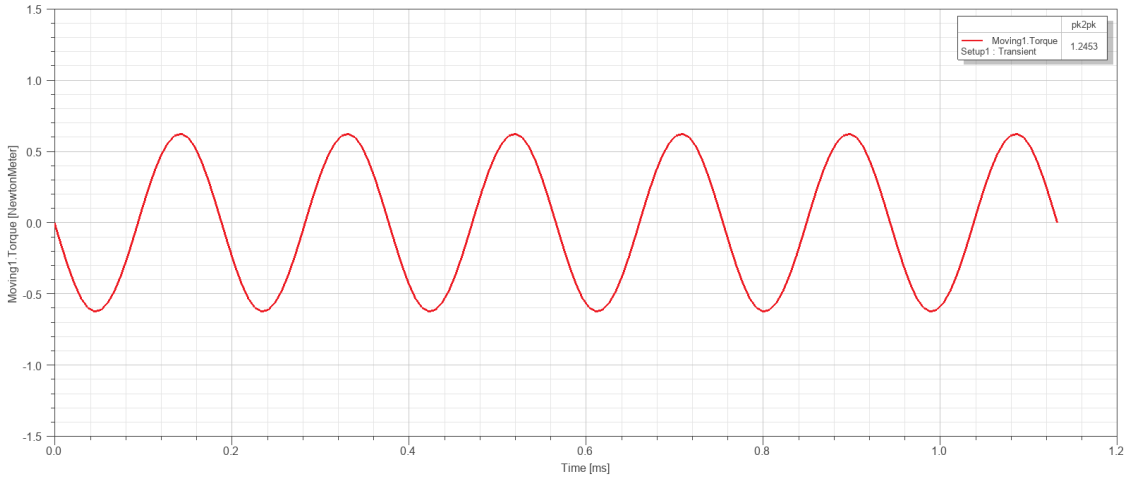

Figure 35. Cogging torque with skew angle.

In figure 36, the static torque is plotted against the current phasor angle αIs. This was produced by running a parametric sweep analysis with angles varying from 0 to 180 degrees with a step magnitude of 10 degrees and a nominal current. The peak torque resulted in approximately 11 Nm. The nominal torque with rated current listed by the manufacturer was 11,1 Nm.

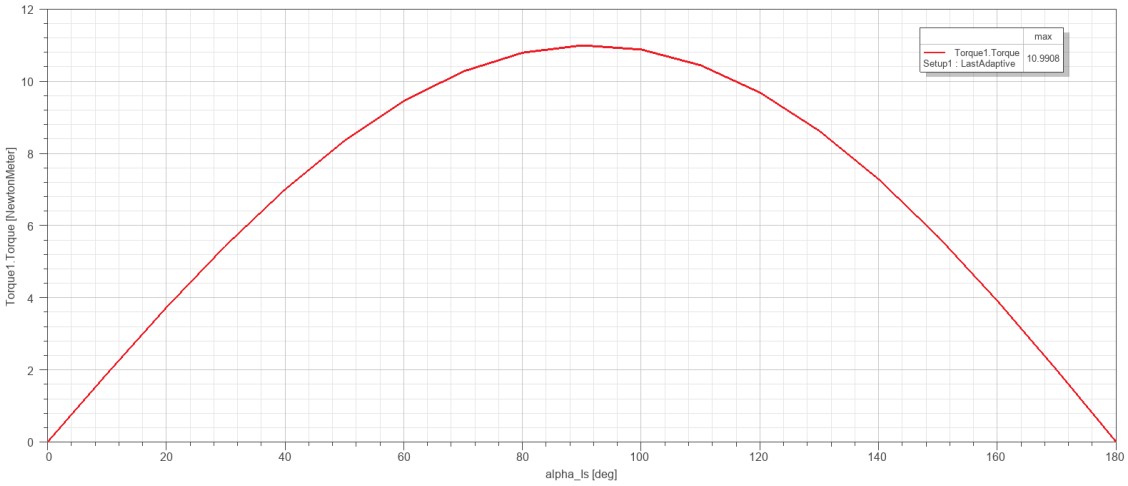

Figure 36. Static torque versus torque angle with rated current.

In figure 37, the induced voltages in each phase can be seen. These were captured with the same transient simulation as were the flux linkages and cogging torque. The rms value was around 227 Volts.

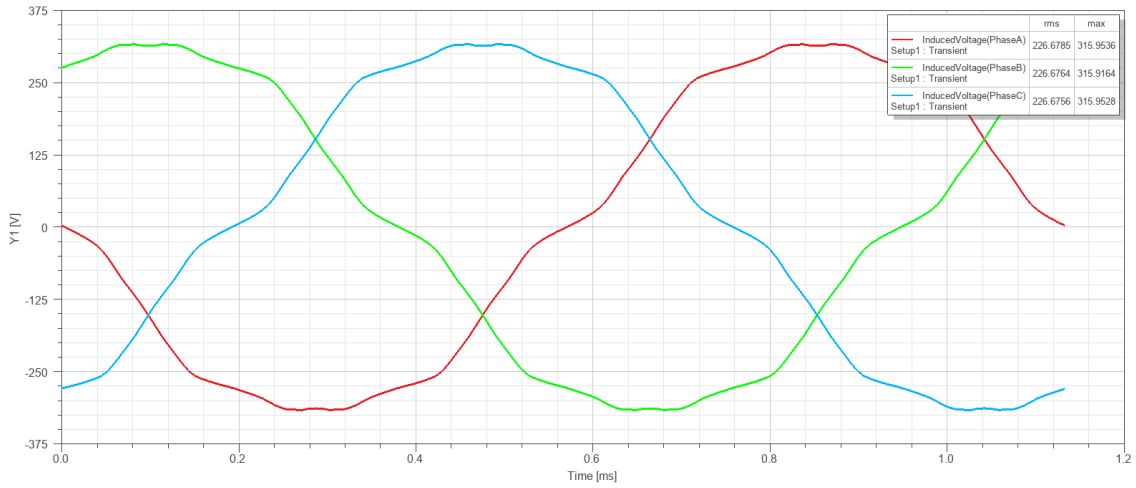

Figure 37. Winding induced voltages with transient setup.

The manufacturer provided the back EMF constant by the value of 0,031 in phase-to-phase rms. With the provided constant, the rms voltage induced at the nominal speed would be approximately 237 V in one phase. So, there was an error of approximately 4%.

In figure 38, the steady state torque produced can be seen. For the steady state torque, the same transient simulation was used as in the back EMF calculation with the addition of the armature current so that the armature field would be created. The current phasor angle αIs used was 90 degrees. The steady state torque resulted in an average value of 10,9 Nm.

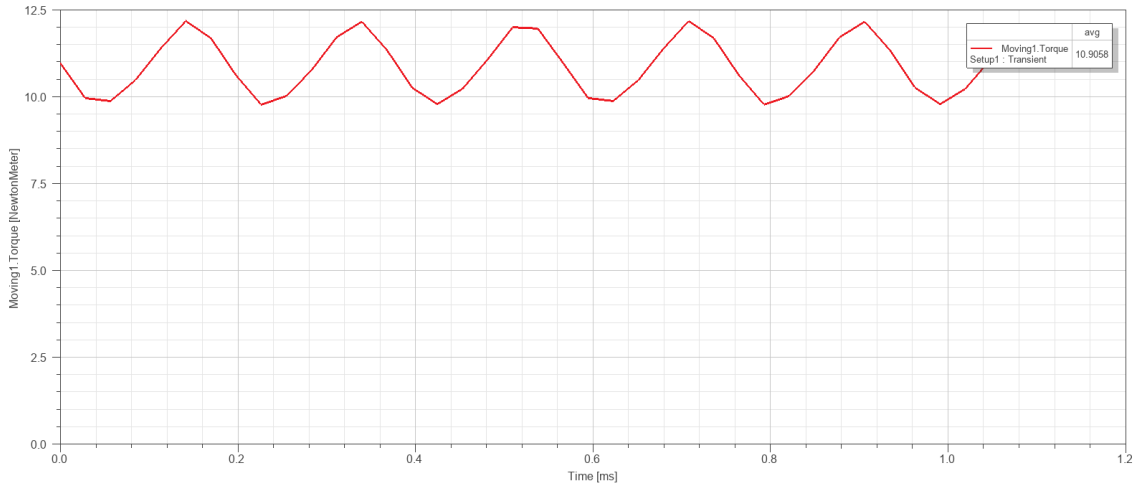

Figure 38. Steady state torque.

In figure 39, the magnetic loading of the motor can be observed. Magnetic loading is the average of the magnitude of the radial flux density around the rotor (Hughes & Drury 2019). This is why the value is obtained as an average absolute, as the direction of flux varies. The simulation gave a value of 0,85 for the magnetic loading. The shape of the plot indicates that it is indeed an 8-pole motor. The smaller jumps on the bottom side of the plot are due to the stator slotting. By observing figure 30, one can see that four of the rotor poles align perfectly with four of the stator teeth, and the other four poles split into two adjacent stator teeth resolving in the shape of the plot.

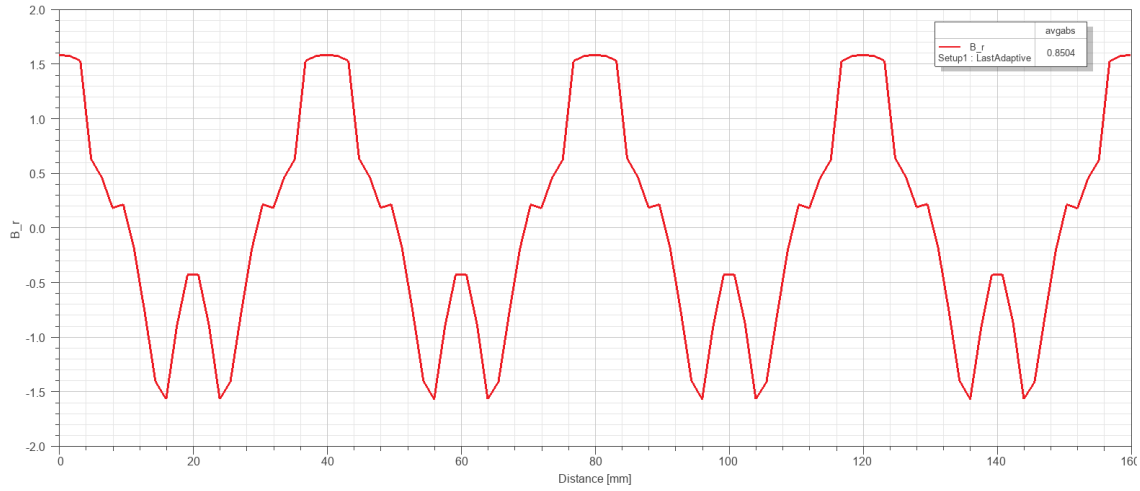

Figure 39. Magnetic field created by permanent magnets.

In figure 40, the magnetic field created by the armature winding is seen. The magnets were removed from the model for this case, so that their magnetic field would have no effect. As can be seen, the created field is very much alike with the field created by the permanent magnets.

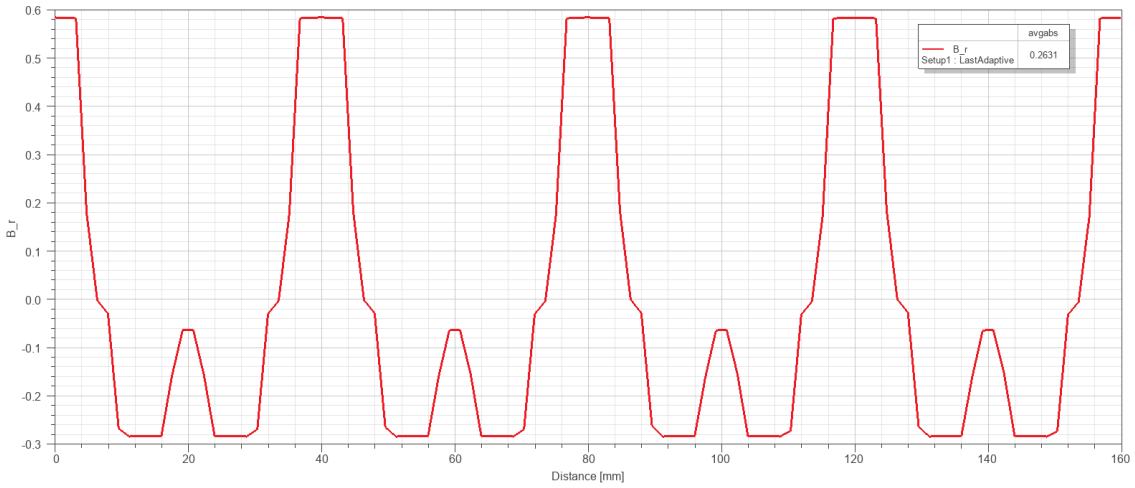

Figure 40. Magnetic field created by armature.

The field was produced by exciting the coils with current. The current equations for each coil were determined through the D- and Q-axis currents as in equations 16, 17 and 18 for phase A, B and C respectively,

$$I_A = I_d \tag{16}$$

$$I_B = -\frac{I_d}{2} + \frac{\sqrt{3}}{2} I_q \tag{17}$$

$$I_C = -\frac{I_d}{2} - \frac{\sqrt{3}}{2} I_q \tag{18}$$

where, Id and Iq are the motor direct- and quadrature axis currents in a phasor diagram. The Id and Iq were defined as in equations 19 and 20,

$$I_d = I_S * \cos(\alpha_{Is}) \tag{19}$$

$$I_q = I_S * \sin(\alpha_{Is}) \tag{20}$$

where Is is the rated coil current and αis is the angle between motor direct axis and stator current axis in the motor phasor diagram.

The current waveforms inputted to the windings can be seen in figure 41 with a rms value of 22,6 A which is exactly the nominal value provided by the manufacturer.

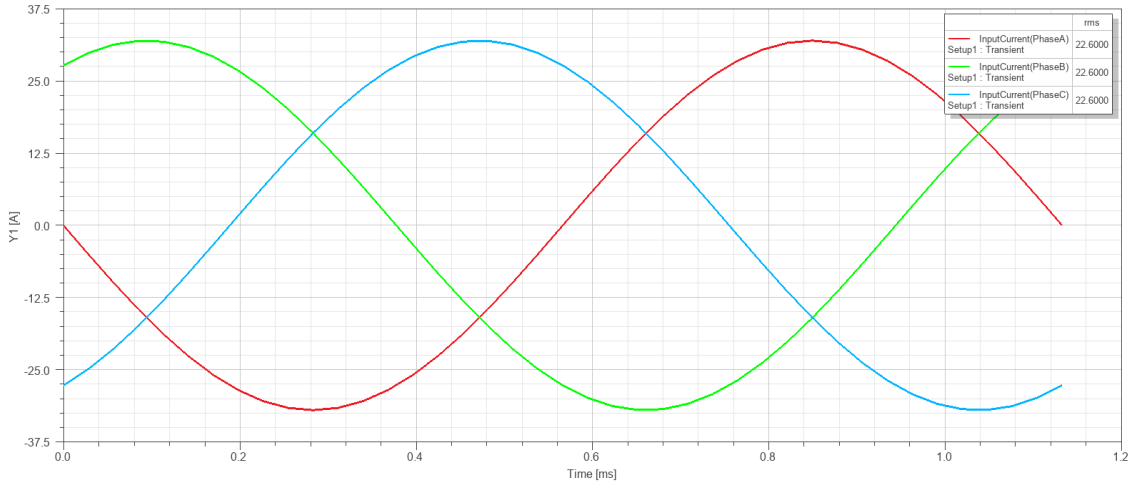

Figure 41. Winding input current.

In figure 42, the core losses are plotted over two electrical time periods. The average is obtained from the second time period, as the losses have a transient state in the first period due to the hysteresis losses. The average was around 187 Watts for total core loss including rotor and stator.

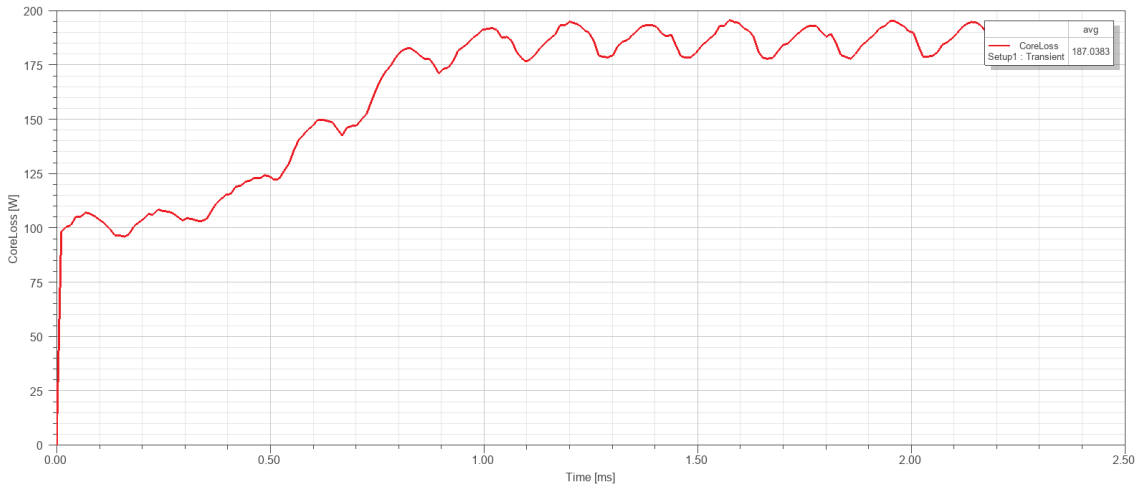

Figure 42. Core losses of rotor and stator over 2 electrical periods.

In figure 43, the copper losses in the windings are plotted. The average value resulted in about 193 Watts.

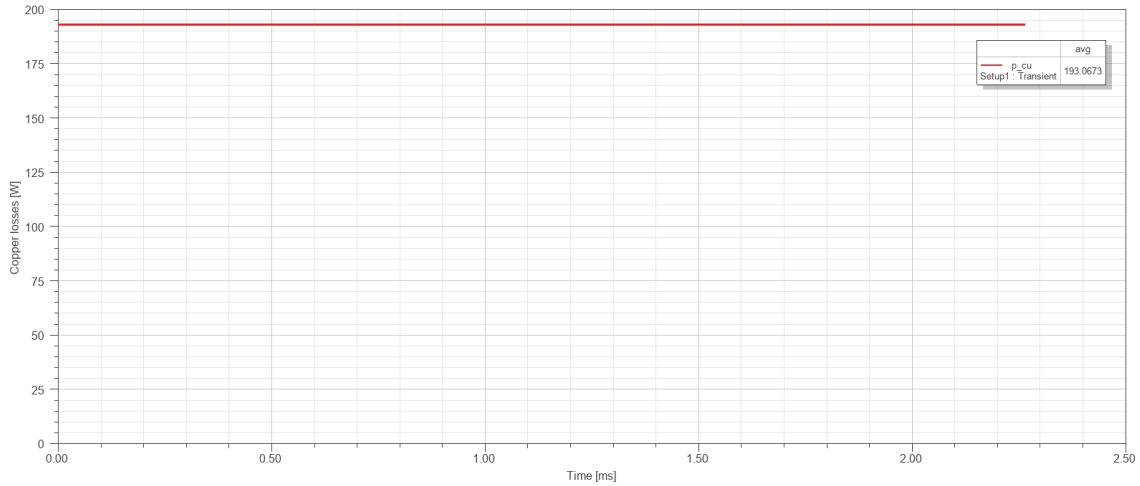

Figure 43. Copper losses.

The copper losses had to be computed by applying the equation 21,

$$P_{cu} = R_{ph} * (I_A^2 + I_B^2 + I_C^2) \quad (21)$$

where Pcu is the total copper loss, Rph is the phase resistance and Ia, Ib and Ic are the phase currents. The motor datasheet states that the winding losses at the nominal speed are 250 Watts, which is significantly higher than what the simulation yielded. This is mainly due to the simulation model, as it is a 2d simulation i.e., it does not consider coil ends nor terminals. The only way to obtain more accurate results is to use a 3D model or alternatively the phase resistance can be adjusted.

The other losses that occur in the motor are eddy currents in the magnets. As the magnets are made of solid material, they are prone to eddy currents, but to calculate these the specific magnet model would have to be known. Thus, they were not included in this thesis. The datasheet states the total losses at the nominal speed to be around 617 Watts and those include winding losses, stator iron losses and rotor losses. Other than those, there are mechanical losses that include bearing friction losses and windage losses due to rotation of the rotor

that can too be computed, but require other Ansys simulation tools like Ansys mechanical and fluent.

7 Data assessment

7.1 Model validity

Overall, the simulation results were very close to the values provided in the data sheets. Essentially all the geometries were inputted with high accuracy and the windings were created corresponding to the real motor. Core material properties were comprehensive allowing the consideration of even more variables than included in this thesis.

The permanent magnets are where the simulation has its weak point. Some of the simulations were done numerous times in search of the magnet that would yield the results closest to the datasheets nominal values. Eventually the closest one found was a neodymium N52 permanent magnet produced by Sura magnets that was found in Ansys's material library. This was used for all of the simulations listed in this thesis.

The model had mostly the same values as listed in the datasheet other than for the induced voltages and the torque. Although the error was relatively small, it was notable nonetheless. The mesh was refined 5 times proving its sufficiency and the simulation time step as well. The only real uncertainty was left in the magnets. As mentioned earlier, as preliminary data was not provided, a VSM would be required to accurately measure the magnetic properties of the magnet.

It is a possibility that the values provided in the datasheet are from analytic calculations i.e., they too can include some error due to parameters not considered in the calculations. Unfortunately, it was not clear from the datasheet if the values were from analytical calculations, simulations or testing.

Excluding the magnets, the model was deemed an accurate representation of the real motor.

7.2 Further development

Two main points of interest lie in the further development of the simulation. The first is the permanent magnet. With an accurate model of the used magnet, the results would undoubtably be more precise as well as the evaluation of losses could be produced for the entire motor. Temperature dependent magnetic properties for the magnets would also be quite crucial for the team, as the motors are under heavy load requiring instant peak torque for acceleration of the vehicle resulting in fairly quick temperature rise. Although the more temperature sensitive part is the inverter, the temperature inside the motor has quite an impact as well.

The second main further development is with the excitation model. As Ansys offers the use of an external circuit allowing the user to build accurate inverter models, there should be no reason not to implement this for the simulation. The implementation was not carried out during the preparation of this thesis because it would have required a significant amount of time and effort, exceeding the intended scope of the project. The accuracy of the inverter model depends largely on the team's knowledge of the specific inverters, similar to motors. However, this can be even more challenging since some internal components cannot be measured, leaving the team reliant on the datasheets provided.

Ansys is compatible with other simulation software such as Simulink. One possibility is that if the team chooses to create its own motor control algorithm, the FEA-model can be exported from Ansys into a Simulink to make the algorithm interact with the created simulation model. This way accurate control is possible compared to using just analytical models.

The simulation can be useful in the design competition the team attends, as in-depth knowledge of the team's vehicle is seen as an advantage. Furthermore, if the team would be interested in designing their own motors, as it has done in the past, the simulation model can be a beneficial comparison or starting point to a completely new motor.

From a mechanical design standpoint, if the model is linked to Ansys mechanical, the bearing loads can be simulated as well, which is one of the team's points of interest as some bearing failures have occurred in the previous seasons. Although this would require the transformation from 2D model to 3D, which is done relatively easily with Ansys Maxwell. In addition, with the 3D model, the losses can be calculated with a more realistic outcome as well, but before moving to 3D environment, the magnet model should be specified.

8 Conclusion

The goal of modelling and simulating an accurate motor FEM-model was mostly achieved. Measurements were executed successfully providing accurate data on necessary geometries in addition to which, material properties were managed to be acquired on top of the elemental composition measurements excluding the permanent magnets.

The results listed in chapter 6 proved to be sufficiently close to the provided values in the motor's datasheet. However, it was concluded that the uncertainty of the permanent magnets properties did cause some error in the results when strictly comparing to datasheet values. The error occurred in the nominal torque and induced voltages, which were on the low side when compared to the datasheet's values. Other possibilities for error were narrowed down by mesh refinement and time step alternation.

To benefit most from the simulation, various possibilities were introduced. Aside from the obvious design material produced for competitions, the model can be implemented to control algorithms if the team chooses to pursue an inhouse

motor control algorithm. For mechanical interests, the model can be introduced to mechanical simulation tools such as Ansys Mechanical to calculate for bearing loads.

Further development ideas and suggestions were also presented with the permanent magnet being the most critical point of interest. For this, a VSM would be required or the manufacturer’s datasheet. 3D environment is one of the easier ones to adopt for more accurate loss calculations and, following that, the inverter model should be implemented with an external circuit for more realistic motor control.

References

Ansys Maxwell. 2025. Ansys. Available from: <https://www.ansys.com/products/electronics/ansys-maxwell>. (accessed on 11 February 2025).

Ansys Maxwell Getting Started. 2020. Ansys. Available from: <https://innovationspace.ansys.com/courses/>. (accessed on 11 February 2025).

Camacho, Juan & Sosa, Victor. 2013. Alternative method to calculate the magnetic field of permanent magnets with azimuthal symmetry. Available from: <https://www.researchgate.net/publication/262707508_Alternative_method_to_calculate_the_magnetic_field_of_permanent_magnets_with_azimuthal_symmetry>. (accessed on 18 February 2025).

Formula Student Rules. 2024. Formula Student Germany. Available from: <https://www.formulastudent.de/fsg/rules/>. (accessed on 10 February 2025).

Gieras, Jacek. 2010. Permanent magnet motor technology. Third edition. CRC Press.

Hughes, Austin & Drury, Bill. 2019. Electric Motors and Drivers. Newnes. Available from: <https://learning.oreilly.com/library/view/electric-motors-and/9780128189252/>. (accessed on 18 February 2025).

IEC 60404-5:2015. Part 5: Permanent magnet (magnetically hard) materials - Methods of measurement of magnetic properties. Available from: <https://standards.iteh.ai/catalog/standards/sist/33ea8d80-9236-4f2c-ae3b-abae24ad951d/sist-en-60404-5-2015>. (accessed on 18 February 2025).

Krings, Andreas & Monissen, Christian. 2021. Review and Trends in Electric Traction Motors for Battery Electric and Hybrid Vehicles. Conference Paper. Available from: <https://www.researchgate.net/publication/344380945_Review_and_Trends_in_Electric_Traction_Motors_for_Battery_Electric_and_Hybrid_Vehicles>. (accessed on 17 February 2025).

Maxwell Help. 2024. Ansys. Software instructional. (accessed on 19 February 2025).

Olympus DS-2000 Specs. 2010. AAATesters. Available from: <https://www.aaatesters.com/olympus-ds-2000-xrf-analyzer-ds2000-olympus-delta.html>. (accessed on 5 March 2025)

Ravi, Teja. 2024. Difference Between Star And Delta Connection. ElectronicsHub. Available from: <https://www.electronicshub.org/comparison-star-delta-connections/>. (accessed on 24 February 2025).

Stacking Factor. 2025. EMETOR. Available from: <https://www.emetor.com/glossary/stacking-factor/>. (accessed on 17 February 2025).